

Falcon: A Remote Sensing Vision-Language Foundation Model

Kelu Yao*, Nuo Xu*, Rong Yang*, Yingying Xu*,
 Zhuoyan Gao, Titinunt Kitrungrotsakul, Yi Ren, Pu Zhang, Jin Wang, Ning Wei, Chao Li 
 Research Center for Space Computing System, ZhejiangLab, Hangzhou, China
 {yaokelu, nuo.xu, yang-rong, cs-ying, lichao}@zhejianglab.org

Abstract

This paper introduces a holistic vision-language foundation model tailored for remote sensing, named Falcon. Falcon offers a unified, prompt-based paradigm that effectively executes comprehensive and complex remote sensing tasks. Falcon demonstrates powerful understanding and reasoning abilities at the image, region, and pixel levels. Specifically, given simple natural language instructions and remote sensing images, Falcon can produce impressive results in text form across 14 distinct tasks, i.e., image classification, object detection, segmentation, image captioning, and etc. To facilitate Falcon’s training and empower its representation capacity to encode rich spatial and semantic information, we developed Falcon_SFT, a large-scale, multi-task, instruction-tuning dataset in the field of remote sensing. The Falcon_SFT dataset consists of approximately 78 million high-quality data samples, covering 5.6 million multi-spatial resolution and multi-view remote sensing images with diverse instructions. It features hierarchical annotations and undergoes manual sampling verification to ensure high data quality and reliability. Extensive comparative experiments are conducted, which verify that Falcon achieves remarkable performance over 67 datasets and 14 tasks, despite having only 0.7B parameters. We release the complete dataset, code, and model weights at <https://github.com/TianHuiLab/Falcon>, hoping to help further develop the open-source community.

1. Introduction

Large vision language models (LVLMs) have demonstrated remarkable success in various vision-language tasks on natural images [1, 12, 38, 55, 101]. However, due to the significant domain and embedded knowledge gap between the natural images and remote sensing images, developing a remote sensing foundational vision-language model remains a substantial challenge. To this end, previous stud-

*: Equal contribution. : Corresponding author.

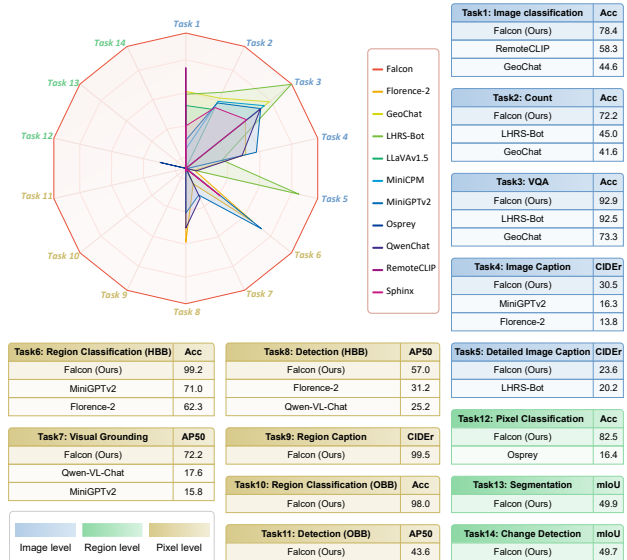


Figure 1. An overall performance comparison between Falcon and 10 state-of-the-art models across 14 remote sensing tasks at image, region, and pixel levels. Results demonstrate that Falcon outperformed existing models, showcasing superior and more comprehensive understanding and reasoning capabilities.

ies [21, 27, 37, 51, 96] usually focused on learning vision-language models that excel in specific remote sensing tasks, limiting their adaptability for more diverse and complex scenarios. With the ongoing advancement of Artificial General Intelligence (AGI) systems, creating a foundational remote sensing model with comprehensive understanding and reasoning capabilities is of significant value.

However, attaining such a foundational remote sensing model still faces significant challenges, which we summarize as follows: 1) Existing models did not feature a universal representation for diverse remote sensing tasks, often failing to facilitate the learning of comprehensive perceptual and reasoning abilities; 2) The absence of a large-scale, high-quality, multi-task dataset for training also limits the ability of current remote sensing models to learn robust and generalized representations.

To address the above challenges, we first propose Falcon,

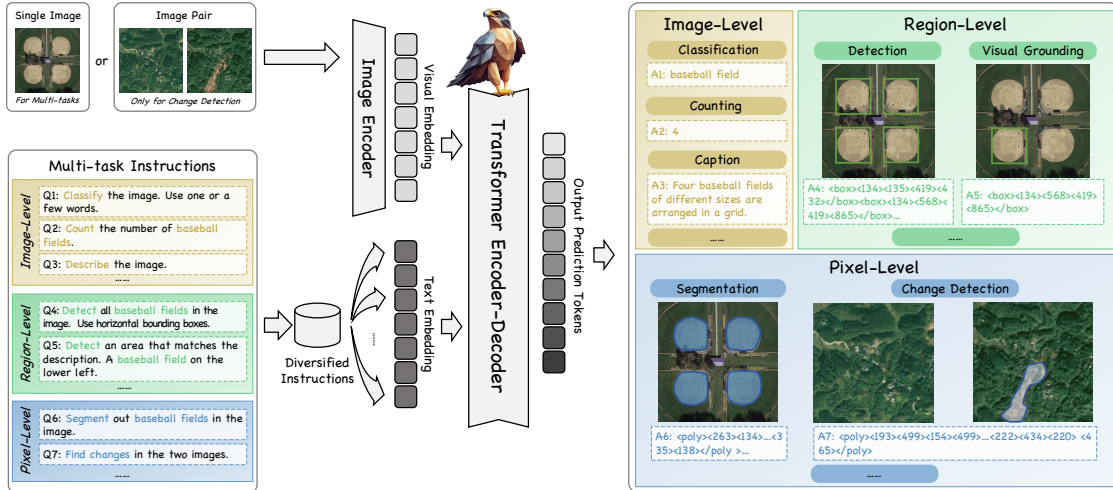


Figure 2. The overview of Falcon model architecture. Given a single image or an image pair (for the task of change detection), Falcon can follow diverse multi-task instructions, generating a universal textual representation suitable for various remote sensing tasks. As shown in the figure, Falcon correctly distinguishes the category of the given image, provides the spatial bounding boxes/segmentations masks for the given objects and even detects subtle changes across images, highlighting its comprehensive capabilities for remote sensing.

a versatile vision-language foundation model with comprehensive perceptual and reasoning abilities tailored for remote sensing. In particular, Falcon features a unified architecture for multitask learning, bridging image-level, region-level, and pixel-level reasoning and understanding abilities in one model. To the best of our knowledge, Falcon is the first remote sensing VLM capable of performing 14 diverse understanding and reasoning tasks across image, region, and pixel levels simultaneously. We hereby provide an ability comparison among various remote sensing VLMs and Falcon in Tab. 1. Compared with Falcon, previous models like GeoChat [27] and RSGPT [21] can only support a limited scope of remote sensing tasks, narrowing their application scenarios.

The crucial challenge for designing Falcon is learning universal representation for diverse remote sensing tasks. Inspired by the latest research in natural image area [74, 77, 81, 91], we utilize a unified network architecture to seamlessly integrate spatial hierarchy and semantic granularity information into a universal representation. The architecture consists of an image encoder and a multi-modality encoder-decoder. This design aligns the vision and language representations, and offers a unified framework to various remote sensing tasks without additional module designs. Besides, to further enhance the instruction understanding capability of Falcon, we propose a dynamic prompt training strategy that leverages multiple differently phrased versions of each instruction. In this way, given user’s prompts and remote sensing images, Falcon can produce results in a unified textual form across a wide range of tasks, *e.g.*, image classification, object detection, segmentation, image captioning, change detection, and etc.

Moreover, to facilitate Falcon’s training, we further

develop Falcon_SFT, a large-scale, multi-task instruction-tuning dataset. Early remote sensing datasets [14, 43, 80] usually focused on a single or a few *vision* tasks. Recent studies proposed *multimodal* remote sensing datasets suitable for training vision-language models. However, these datasets often contain a limited number of image-text pairs, making them only useful for training models on specific tasks [21, 89, 96]. Therefore, we present Falcon_SFT, a large-scale multi-task instruction-tuning dataset. The Falcon_SFT dataset consists of approximately 78 million high-quality data samples, covering 5.6 million multi-spatial resolution and multi-view remote sensing images. Specifically, we uniformly standardize each sample in the Falcon_SFT dataset into a unified format, facilitating the training of our proposed Falcon. Please see Fig. 3 for data examples.

In experiments, we conduct a variety of evaluations of our proposed Falcon both qualitatively and quantitatively (see Fig. 1 for a quick preview). For qualitative evaluations, we visualize the prediction results of 14 tasks individually and compare with other state-of-the-art methods, in order to evaluate the performance of Falcon. For quantitative evaluations, we assess the performance of Falcon on each downstream task, along with its zero-shot performance on unseen data samples, highlighting the generalization ability of Falcon. Beside, we conduct detailed ablation studies for Falcon, showcasing the effectiveness of our training recipes.

Finally, to address the critical absence of a high-performance foundational model for remote sensing in the community, we will fully *open-source* our work with complete dataset, code and model weights, aiming to bridge the gap between foundational models for remote sensing imagery and foundational models for natural imagery. Despite the substantial financial investment of our proposed Falcon,

	Models	Image level					Region level						Pixel level		
		Cls	Cap	D. Cap	Count	VQA	Cls ^{hbb}	Cls ^{obb}	R.Cap	Det ^{hbb}	Det ^{obb}	VG	Cls ^{poly}	Seg	CD
Remote Sensing VLMs	GeoChat[27]	✓	✓	✓	✓	✓			✓			✓			
	GeoRSCLIP[96]	✓								✓		✓		✓	
	LHRS-Bot[51]	✓	✓	✓	✓	✓				✓		✓			
	RemoteCLIP[37]	✓				✓									
	SkyCLIP[75]	✓													
	RSGPT[21]	✓	✓		✓	✓									
	GRAFT [49]	✓	✓	✓	✓	✓								✓	
	EarthGPT[93]	✓	✓	✓	✓	✓			✓	✓	✓	✓			
	RS-ChatGPT [17]	✓	✓	✓	✓	✓								✓	
	SkyEyeGPT[89]	✓	✓	✓	✓	✓						✓			
	RS-CapRat [64]	✓	✓	✓	✓	✓								✓	
	Popeye [92]		✓	✓	✓	✓				✓	✓			✓	
	MGIMM [83]		✓	✓	✓	✓			✓						
	EarthMarker [94]	✓	✓	✓	✓	✓	✓		✓	✓			✓		
	Falcon(Ours)	✓	✓	✓	✓	✓	✓	✓	✓	✓	✓	✓	✓	✓	✓

Table 1. Comparisons of capabilities of different remote sensing vision-language models. Several representative models have been included in this table. Notably, Falcon exhibits the most comprehensive understanding and reasoning capabilities, covering image, region, and pixel levels comprehensively. For task abbreviations in the second row, please see Fig. 3 for details.

we hope this effort will foster further research and development in the field, advancing the capabilities of remote sensing models and their real-world applications.

Contributions of this paper can be summarized as follows. 1) To the best of our knowledge, Falcon is the first remote sensing vision-language model to feature image, region, and pixel-level understanding and reasoning capabilities, supporting 14 tasks within a unified architecture. 2) As of March 2025, Falcon_SFT stands as the largest and most comprehensive dataset for training vision-language models in the remote sensing field. 3) We have conducted extensive experiments to demonstrate the superiority of Falcon over previous VLMs, highlighting the effectiveness of Falcon and Falcon_SFT in the field of remote sensing. The complete dataset, code, and model weights will be fully open-sourced to the community.

2. Related work

2.1. Remote sensing datasets

The development of high-quality remote sensing datasets has attracted increasing attention in recent years. Previous studies on this field mainly focused on two perspectives. Some studies [14, 34, 67, 80] focused on image datasets each targeting a single or a few vision tasks. Long *et al.* [43] proposed Million-AID, a large-scale image dataset containing 51 categories and a million instances for remote sensing scene classification. G. Sumbul *et al.* [65] introduced BigEarthNet, comprising 590,326 images collected from Sentinel-1 and Sentinel-2 satellites, featuring several resolutions and image sizes. The DOTA series datasets [14, 80] were mainly sourced from Google Earth, the GF-2 satellite, and aerial images, which have greatly advanced the field of object detection. The latest version [14] featured 11,268 images, 18 categories, and an extensive set of annotations with oriented bounding boxes. Jacob Shermeyer *et*

Dataset	Rep.VLM	#Images	#Annotations	#tasks	Spatial hierarchy
RSSM	GeoRSCLIP [96]	-	5M	1	Image-level
LHRS-Align	LHRS-Bot [51]	1.15M	1.15M	1	Image-level
RSICap	RSGPT [21]	2192	2192	1	Image-level
MMRS-1M	EarthGPT [93]	-	1M	5	Image & Region-level
SkyEye-968k	SkyEyeGPT [89]	-	968k	4	Image & Region-level
RSVP-3M	EarthMarker [94]	-	3M	5	Image & Region-level
Falcon_SFT(Ours)	Falcon(Ours)	5.6M	78.2M	14	Image & Region & Pixel-level

Table 2. Comparisons with VLMs’ remote sensing datasets.

al. [61] proposed RarePlanes dataset in order to improve the performance of detecting aircraft and their attributes in satellite imagery. GID [69], UAVid[45], DLRSD[59] were commonly used datasets for the semantic segmentation task of RGB remote sensing images.

Besides, several studies [40, 44, 86, 88] have developed multimodal datasets to support vision-language models in remote sensing. Dilxat Muhtar *et al.* [51] developed LHRS-Align, which included 0.9K samples for visual reasoning, 4K samples for detailed image descriptions, and 7K samples for conversational tasks. However, to use this dataset, users must download the original images from Google Earth imagery. RSICD [44], Sydney-Captions [54], UCM-Captions [54], NWPU-Captions [9] were datasets specifically created for remote sensing image caption generation tasks, containing 10921, 613, 2000, 31500 images, each accompanied by descriptions of varying lengths.

Despite previous advancements, existing remote sensing datasets remained limited in terms of data scale, task diversity, hierarchical annotation, and annotation quality. The field still lacked a large-scale, multi-task dataset suitable for training foundational vision-language models, hindering their progress. To address this challenge, we present Falcon_SFT in this paper, a comprehensive, large-scale, multi-task instruction-tuning dataset for remote sensing. Specifically, we compiled 67 remote sensing datasets covering a variety of tasks, please refer to supplementary material for details.



Figure 3. An illustrative example of images, their corresponding instructions, and output format of different tasks in Falcon_SFT dataset.

2.2. Remote Sensing Foundation Models

Recently, a considerable literature has grown up around the theme of developing remote sensing foundation models. These pre-trained foundation models can be categorized based on architectural design. The first category consists of ViT-based vision foundation models [35, 48, 50, 56]. For instance, Sun *et al.* proposed RingMo [66], a classic remote sensing vision model fine-tuning on 4 downstream tasks. These methods lacked reasoning abilities and cannot be controlled via natural language instructions. The second category includes CLIP-based vision-language models [37, 75, 96]. For instance, Liu *et al.* proposed RemoteCLIP [37], the first vision-language foundation model for remote sensing that aligned text embeddings for downstream application. However, these methods cannot perform dif-

ferent tasks without designing additional modules. The third category comprises LLM-based vision-language models [27, 51, 92, 93]. Zhan *et al.* proposed SkyEyeGPT [89], specifically designed for remote sensing images understanding. Kartik Kuckreja *et al.* [27] introduced GeoChat, a versatile LLaVA-based remote sensing vision-language model, but it cannot perform complex pixel-level tasks such as segmentation or change detection. Similarly, LHRs-Bot [51] also lacked such capabilities. Furthermore, these methods often exceeded 7 billion parameters, leading to computational bottlenecks and low inference efficiency when deployed on edge devices. More importantly, we believe that the LLMs module containing significant number of parameters may not play an essential role in remote sensing, considering that this task still primarily focuses on the visual

input. Therefore, in this paper, we propose a lightweight vision-language model to efficiently handle various remote sensing tasks in a unified paradigm.

3. Algorithm

In this section, we aim to delve into the details of Falcon, introducing a simple yet effective way to address challenges of unifying many complex remote sensing tasks in one manner. Specifically, we will introduce the design of Falcon’s architecture and a multi-task learning paradigm, that enables the unification of various vision-language tasks.

Notation: Let $\mathcal{I} \in \mathbb{R}^{H \times W \times 3}$ denote the input remote sensing image, with H and W denoting the height and width of the image. \mathcal{T} denotes the input textual prompt. y denotes the prediction target *i.e.*, the formulated visual annotations. \mathcal{G} denotes the image encoder. \mathcal{E} denotes the text token embedding function. \mathcal{F} denotes the standard encoder-decoder network of the transformer architecture.

In Falcon, we employ a sequence-to-sequence framework that is capable of putting all distinct tasks in a unified format. As depicted in Fig. 2, given a remote sensing image \mathcal{I} and a text prompt \mathcal{T} , we feed \mathcal{I} to image encoder \mathcal{G} to extract the visual token embedding $\mathcal{V} \in \mathbb{R}^{N_v \times D_v}$, with N_v and D_v respectively represent the number and dimension of vision tokens. At the same time, we leverage \mathcal{E} to process \mathcal{T} in order to obtain the text token embedding $\mathcal{E}(\mathcal{T}) \in \mathbb{R}^{N_t \times D}$. Next, we combine the vision token embedding and the text token embedding to form a multi-modality embedding $\mathcal{X} = [\mathcal{V}', \mathcal{E}(\mathcal{T})]$, with $\mathcal{V}' \in \mathbb{R}^{N_t \times D}$ is derived from \mathcal{V} through a visual adapter [81], serving as the task-agnostic input to \mathcal{F} .

Unlike the previous studies [27, 81], we propose a dynamic prompt training strategy to eliminate the reliance on task-specific tokens. Specially, given a prompt \mathcal{T} , Falcon will dynamically sample several differently phrased versions $\{\mathcal{T}'_i\}_{i=1}^M$ from a predefined prompt pool to form the $\mathcal{X} = \{[\mathcal{V}', \mathcal{E}(\mathcal{T}'_i)]\}_{i=1}^M$ to join the training process. Note that $\{\mathcal{T}'_i\}_{i=1}^M$ and \mathcal{T} share similar semantic meanings. This design further enhances Falcon’s understanding ability of natural language.

To ensure the input and output of distinct tasks in a unified format, we treat each task as a sequence-to-sequence translation task. As shown in Fig. 3, we regard images, prompts, annotations as special languages. For example, an instruction of unified format for the region caption is as follows: "Describe the $\langle region \rangle$ in the image.", where $\langle region \rangle$ is $\langle box \rangle \langle x1 \rangle \langle y1 \rangle \langle x2 \rangle \langle y2 \rangle \langle /box \rangle$ representing location tokens. The location tokens are the coordinates of the bounding box. We add location tokens to the tokenizer’s vocabulary list, representing quantized coordinates. We create 1000 bins which represent regions using formats tailored to task requirements.

Loss function. We utilize the cross-entropy loss to optimize

the Falcon for 14 tasks like normal large language models.

$$\mathcal{L} = - \sum_{i=1}^{|y|} \sum_{x \in \mathcal{X}} \log P_{\theta}(y_i | y_{<i}, x), \quad (1)$$

where $x \in \mathcal{X}$ is the input vector consisting of the image embedding output by the image encoder and the prompt embedding; y is the prediction target; $|y|$ is the number of target tokens, θ is the Falcon’s parameter.

4. Dataset

To equip Falcon with powerful image, region, and pixel-level understanding and reasoning capabilities, we introduce Falcon_SFT, the first large-scale, multi-task remote sensing instruction-tuning dataset. It contains 78 million high-quality samples covering 5.6 million multi-resolution, multi-view remote sensing images. This section details its creation process, including data collection, preprocessing, and instruction generation.

4.1. Data Collection and Preprocessing

Currently, no existing dataset can fully meet the training requirements of Falcon. To address this, we devised a simple and straightforward approach, *i.e.* curating and combining various open-source datasets in remote sensing filed.

We collected 90 annotated task-specific RGB image datasets, such as Million-AID [43], RSICD [44], and DOTA [14, 80], encompassing nearly all publicly available datasets originating from satellites, airplanes, drones, etc. After manual screening, we refined the selection to 67 relevant datasets. The complete list is available in Sec. A of the supplementary material. Notably, we provide download links and metadata (image size, spatial resolution, and quantity) to help reduce data collection efforts for researchers.

Next, we integrate the 67 collected remote sensing datasets, by establishing a unified and consistent annotation format. This standardization is necessary because different datasets use varying annotation formats (e.g., polygons vs. mask images), which can complicate data integration. Besides, to broaden application scenarios, we repurpose existing data structures to generate additional annotations, expanding the number of supported tasks to 14. These tasks are categorized into three levels, namely, *Image-level*: Image Classification, Image VQA, Counting, Image Captioning, and Image Detailed Captioning; *Region-level*: Region Classification-HBB, Region Classification-OBB, Region Detection-HBB, Region Detection-OBB, Visual Grounding, and Region Captioning; *Pixel-level*: Pixel Classification, Pixel Segmentation, and Change Detection. This categorization aligns with prior discussions in [77, 91]. For more detailed data collection and preprocessing procedures, please see Sec. A of the supplementary material.

		Accuracy																												
Models	#params	BHP Watertranks	CLRS	DIOR	DOTA2.0	FAIRMI.0	GEONRW	Globe230k	Hefei	Hurricane-Damage	LoveDA	MultiScene	NWPU-RESISC45	NASC.TG2	OPTIMAL31	AIRound	PatternNet	RSD46.WHU	RSITMD	RSLCB	RSOD	RSSCN7	RS.C11	SIRLWHU	SODA-A	UCAS-AOD	WHU_GID	ISAID	million-AID	xView
MiniCPM-V[20]	3B	0.06	0.14	0.08	0.10	0.12	0.03	0.07	0.13	0.14	0.06	0.03	0.15	0.12	0.17	0.11	0.14	0.10	0.14	0.09	0.25	0.16	0.15	0.10	0.08	0.36	0.09	0.12	0.11	0.02
MiniGPT-v2[101]	7B	0.03	0.26	0.16	0.11	0.06	0.03	0.05	0.11	0.12	0.06	0.06	0.31	0.08	0.36	0.43	0.34	0.16	0.30	0.19	0.03	0.27	0.18	0.12	0.05	0.02	0.32	0.11	0.25	0.12
LLaVA-1.5[38]	7B	0.28	0.44	0.35	0.19	0.33	0.17	0.31	0.29	0.41	0.15	0.15	0.46	0.31	0.56	0.54	0.47	0.36	0.47	0.31	0.44	0.50	0.48	0.36	0.34	0.52	0.59	0.24	0.30	0.24
Qwen-VL-Chat[3]	7B	0.11	0.33	0.17	0.10	0.12	0.09	0.23	0.18	0.20	0.05	0.07	0.32	0.17	0.40	0.41	0.34	0.20	0.30	0.15	0.27	0.39	0.41	0.12	0.11	0.42	0.53	0.13	0.27	0.09
Sphinx[36]	7B	0.21	0.22	0.18	0.13	0.34	0.08	0.18	0.23	0.33	0.11	0.09	0.24	0.24	0.29	0.27	0.26	0.13	0.21	0.14	0.81	0.26	0.33	0.24	0.21	0.69	0.37	0.19	0.08	0.06
RemoteCLIP [37]	304M	0.40	0.64	0.59	0.46	0.54	0.36	0.37	0.37	0.40	0.60	0.30	0.68	0.57	0.78	0.60	0.60	0.44	0.81	0.46	0.98	0.67	0.69	0.57	0.56	0.99	0.87	0.59	0.44	0.38
GeoChat[27]	7B	0.56	0.46	0.65	0.60	0.70	0.12	0.20	0.21	0.38	0.11	0.10	0.58	0.36	0.62	0.59	0.48	0.29	0.46	0.29	0.94	0.36	0.51	0.32	0.60	0.91	0.53	0.54	0.38	0.29
LHRS-Bot[51]	7B	0.28	0.58	0.35	0.20	0.33	0.16	0.25	0.21	0.17	0.16	0.14	0.73	0.49	0.87	0.56	0.59	0.38	0.74	0.39	0.54	0.55	0.72	0.44	0.28	0.55	0.76	0.23	0.37	0.23
Falcon(Ours)	0.7B	0.98	0.91	0.87	0.95	0.98	0.90	0.71	0.79	0.99	0.56	0.57	0.94	0.99	0.97	0.85	0.99	0.56	0.50	0.99	0.99	0.94	0.92	0.96	0.88	1.00	0.95	0.89	0.93	0.85

Table 3. A comparison of image classification performance on several datasets with 8 generic and remote sensing VLMs.

		Accuracy														
Models	#params	ASD	DIOR	DOTA2.0	FAIRMI.0	RSVQA HR	HRSC2016	RSOD	S2-SHIPS	SODA-A	ShipRS	UCAS-AOD	VHRShips	airplane_det	ship_det	xView
MiniCPM-V[20]	3B	0.662	0.426	0.260	0.295	0.281	0.599	0.302	0.031	0.161	0.555	0.321	0.777	0.360	0.707	0.132
MiniGPT-v2[101]	7B	0.637	0.429	0.248	0.336	0.275	0.595	0.295	0.063	0.148	0.527	0.293	0.768	0.306	0.659	0.152
LLaVA-1.5[38]	7B	0.681	0.249	0.221	0.268	0.000	0.478	0.326	0.125	0.175	0.371	0.400	0.683	0.453	0.561	0.101
Sphinx[36]	7B	0.480	0.430	0.257	0.365	0.181	0.669	0.403	0.031	0.151	0.516	0.388	0.741	0.384	0.195	0.146
GeoChat[27]	7B	0.738	0.453	0.240	0.377	0.240	0.588	0.302	0.156	0.165	0.545	0.308	0.774	0.466	0.683	0.171
LHRS-Bot[51]	7B	0.678	0.455	0.244	0.357	0.681	0.714	0.319	0.125	0.171	0.611	0.362	0.773	0.371	0.732	0.170
Falcon(Ours)	0.7B	0.952	0.770	0.619	0.816	0.718	0.838	0.821	0.156	0.391	0.782	0.857	0.916	0.808	0.854	0.278

Table 4. A comparison of object number counting performance on several datasets with both generic and remote sensing VLMs.

4.2. Unified Instruction Generation

Next, we transform our integrated dataset into a multi-task instruction-tuning dataset for vision-language model training. We take the steps as follows.

Define Instruction Templates. To facilitate the understanding and execution of specific tasks by VLMs, we design standardized instruction templates based on different remote sensing tasks. For examples, for the Object Detection Task, “Detect *<class>* in the image. Use Rotated bounding boxes.” is given. The rotated bounding box is represented as *<quad>* *<x₁>* *<y₁>* *<x₂>* *<y₂>* *<x₃>* *<y₃>* *<x₄>* *<y₄>* *</quad>*, specifying the coordinates of the four vertices, each expressed in thousandths. Please see Fig. 3 for instruction examples of all 14 tasks.

Generate Image Instruction Pairs. To create image instruction pairs based on the defined templates, we first iterate over the dataset and generate specific instruction for each image based on its task type (*e.g.*, detection, segmentation). We then combine the generated instruction with corresponding image and annotations into a structured pair. This enables the model to learn diverse task responses using different instruction-based prompts.

Generate the Multi-instruction Pool. To enhance language understanding and reduce reliance on task-specific tokens, we diversify instruction patterns for each task using an LLM [2]. It generates multiple variations of the same instruction with different complexity levels. For instance, “Describe the image.” is expanded into “Describe

the contents of this image.”, “Analyze the image and explain its visual content.”, and “Can you identify what this image shows?”. This approach enriches textual diversity in training data, helping VLMs to improve performance across various tasks. Please see Sec. B of the supplementary material for multi-instruction examples.

4.3. Falcon_SFT Dataset

Following the above data processing steps, we finally constructed the large-scale remote sensing instruction-tuning dataset Falcon_SFT. We compare Falcon_SFT with various datasets used for remote sensing vision-language models in Tab. 2. The Falcon_SFT dataset features the largest number of samples (78 million) and images (5.6 million), supporting the highest number of tasks (14). It is also more comprehensive by covering image, region, and pixel-level spatial hierarchies. For detailed statistics of Falcon_SFT dataset, please see Tab. II in Sec. A of the supplementary material.

5. Experiments

In this section, we present the experimental setup and results to evaluate Falcon’s performance, including: 1) both qualitative and quantitative performance evaluations on all 14 complex remote sensing tasks; 2) zero-shot performance of Falcon compared with previous methods. The results demonstrate Falcon’s ability to handle complex vision-language tasks and highlight its strengths in image, region, and pixel-level understanding and reasoning. To point out,

Models	#params	RSVQA HR(Accuracy)	
		Compare	presence
MiniCPM-V[20]	3B	0.734	0.646
MiniGPT-v2[101]	7B	0.647	0.668
Qwen-VL-Chat[3]	7B	0.668	0.643
Florence-2-L[81]	0.7B	0.396	0.650
Sphinx[36]	7B	0.556	0.514
GeoChat[27]	7B	0.778	0.688
LHRS-Bot[51]	7B	0.922	0.928
Falcon(Ours)	0.7B	0.927	0.931

Table 5. A comparison of VQA performance on several datasets with 7 generic and remote sensing VLMs.

Rank	Detail				Position				Hallucination			
	GeoChat	Qwen	Sphinx	Falcon	GeoChat	Qwen	Sphinx	Falcon	GeoChat	Qwen	Sphinx	Falcon
A=4	7	45	92	196	15	38	75	148	47	290	161	280
B=3	101	170	240	250	106	110	163	207	95	137	197	159
C=2	295	218	154	49	328	188	221	136	170	53	121	55
D=1	97	67	14	5	51	164	41	9	188	20	21	6
Average	2.036	2.386	2.82	3.274	2.17	2.044	2.544	2.988	2.002	3.39	2.996	3.426

Table 6. A comparison of human evaluations for image captioning. Each value in 3-6 rows represents the number of captions marked as A/B/C/D by 10 volunteers. We calculated the average score in the last row, by quantifying the A-D ratings as 4 to 1 points.

due to the page limit, we provide additional experimental results in the supplementary material, including qualitative performance evaluations of all 14 tasks in Sec. E, quantitative performance evaluations for tasks not covered in the main paper in Sec. F, qualitative performance evaluations on diversified instructions in Sec. G, human evaluations on image captioning performance in Sec. H, more ablation studies in Sec. I and the details of evaluation metrics for each task in Sec. J.

Implementation Details. Falcon consists of an image encoder and a transformer-based encoder-decoder, with a total of 0.7B parameters. The detailed architecture is illustrated in Fig. 2. We initialized the model’s parameters using the pre-trained weights provided by [81]. Unlike [81], we increased the output token length to 4096 in order to obtain more detailed representations. The training batch size for Falcon was 640, the learning rate was set to $1e^{-5}$, and the image size is 448×448 . We trained the model for 4 days using 160 Nvidia A100 GPUs.

5.1. Performance Evaluation across 14 tasks

Image-level Tasks. In this section, we presented the performance of Falcon over image classification tasks (*c.f.* Tab. 3), counting tasks (*c.f.* Tab. 4) and VQA tasks (*c.f.* Tab. 5). As shown in Tab. 3, generic VLMs, such as MiniGPTv2 [101] and Qwen_chat [3] encountered obstacles in performing effectively on remote sensing data, since they usually lacked the expert knowledge of this domain. Meanwhile, compared with VLMs specialized in remote sensing [27, 37, 51], Falcon achieved better performance in all related datasets, with only 0.7B parameters. Besides, we also provided detailed performance comparison of counting targets in Tab. 4. Such a task requires compositional perception and reasoning capabilities, presenting significant

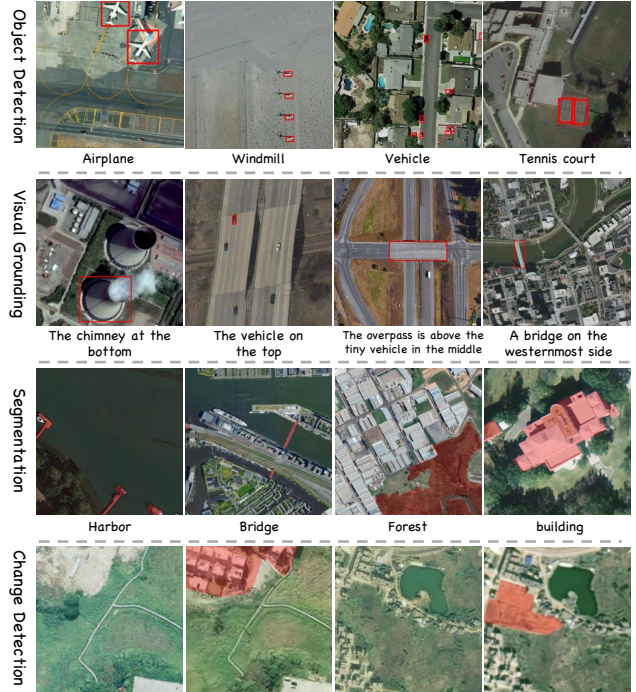


Figure 4. Visualization of Falcon’s output on tasks of object detection, visual grounding, segmentation, and change detection.

challenges to state-of-the-art VLMs. To this end, Falcon achieved superior performance in targets counting, showcasing its sophisticated capabilities. Finally, we compared Falcon with previous VLMs in VQA tasks, which these models usually excelled in. As shown in Tab. 5, Falcon still surpassed previous VLMs with less model parameters, indicating its strong instruction following capabilities.

For image captioning tasks, we conduct human evaluations for Falcon’s responses. Specifically, captions were evaluated across three dimensions: detail, position, and hallucination, using a four-level rating system (*i.e.*, A, B, C, D quantified as 4 to 1 points, where a higher point represents a better caption). The results in Tab. 6 showed that Falcon achieved the highest average scores across all three dimensions, compared with other VLMs. Please see Sec. H of the supplementary material for detailed experimental setup.

Region-level Tasks. Beyond image-level tasks, our Falcon also support fine-grained region-level tasks. To this end, we present the performance of Falcon on object detection (horizontal bounding box) in Tab. 7. It is noticeable that previous VLMs demonstrated limited performance in this task, exposing their limitations in localization capabilities. In contrast, Falcon outperformed previous methods, highlighting its ability to handle complex remote sensing tasks.

Pixel-level Tasks. Besides, we also present the evaluation results of Falcon on pixel-level tasks. To the best of our knowledge, Falcon is the first VLM capable of showing satisfactory performance on pixel-level tasks, such as seg-

Models	#params	AP@IoU=0.5(%)											
		BHP Watertanks	DIOR	DOTA2.0	GEONRW	Globe230k	HRSC2016	LoveDA	RSOD	UCAS-AOD	VHRShips	iSAID	xView
MiniGPTv2 [101]	7B	7.228	9.430	1.624	2.085	14.456	51.156	15.769	24.564	34.944	42.896	2.535	0.722
Florence-2-L [81]	0.7B	5.810	26.975	12.245	0.410	8.971	67.159	8.484	62.750	78.792	66.883	16.673	3.259
Qwen-VL-Chat [3]	7B	9.795	15.807	2.970	2.672	12.106	58.547	18.989	38.906	53.929	53.393	4.292	1.561
Sphinx [36]	7B	0.068	0.469	0.054	0.572	5.780	3.866	4.481	0.292	0.021	0.537	0.111	0.014
Falcon(Ours)	0.7B	81.896	56.652	27.043	30.410	30.458	93.750	47.214	85.249	93.838	89.543	33.846	27.165

Table 7. A comparison with generic and remote sensing VLMs on object detection with horizontal bounding box.

Models	#params	Image level				Region level			Pixel level		
		Cap (CIDEr)		D.Cap (CIDEr)		Count(%) (Acc)		Det ^{hbb} (%) (AP@IoU=0.5)	Cls ^{hbb} (%) (Acc)	Seg (mIoU)	CD (mIoU)
		UCM-Captions	UCM-Captions	MAR20	NWPU-VHR-10	MAR20	NWPU-VHR-10	NWPU-VHR-10	GID15	CCD	WHU-CD
		MiniCPM-V [20]	3B	0.000	0.000	39.1	48.1	-	-	-	-
MiniGPT-v2 [101]	7B	16.282	0.166	35.4	49.9	53.078	22.828	76.5	-	-	-
LLaVA-1.5 [38]	7B	0.004	0.010	47.5	34.4	-	-	-	-	-	-
Qwen-VL-Chat [3]	7B	12.992	1.912	-	-	79.286	32.099	-	-	-	-
Florence-2-L [81]	0.7B	13.844	1.568	-	-	88.843	38.905	52.9	-	-	-
Sphinx [36]	7B	0.000	0.056	45.8	50.1	0.161	0.185	35.9	-	-	-
GeoChat [27]	7B	0.288	0.092	42.3	43.6	-	-	-	-	-	-
LHRS-Bot [51]	7B	8.365	20.180	40.6	48.7	-	-	-	-	-	-
Falcon(Ours)	0.7B	30.481	23.553	87.6	81.7	94.025	81.847	98.8	0.389	0.427	0.531

Table 8. A comparison of zero-shot performance on various tasks with 8 generic and remote sensing VLMs.

Data scale	Task granularity			#params	Image level			Region level		Pixel level	
	Image level	Region level	Pixel level		Cap (CIDEr)	D.Cap (CIDEr)	Count(%) (Acc)	Det ^{hbb} (%) (AP@IoU=0.5)	Cls ^{hbb} (%) (Acc)	Seg (mIoU)	CD (mIoU)
	10%	✓	✓		✓	0.7B	74.3	15.1	58.2	38.4	98.4
50%	✓	✓	✓	0.7B	94.7	26.3	60.7	42.6	93.7	0.524	0.514
-	✓	✗	✗	0.7B	96.7	25.9	61.6	0.0	75.0	0.042	0.000
-	✓	✓	✗	0.7B	97.2	24.8	63.2	36.0	99.3	0.042	0.000
100%	✓	✓	✓	0.3B	107.6	25.6	64.4	42.8	97.7	0.529	0.542
100%	✓	✓	✓	0.7B	111.4	27.9	65.2	43.3	99.2	0.544	0.536

Table 9. Ablation studies on the effects of data scale, task granularity, and model size for Falcon.

mentation and change detection. The qualitative results of Falcon are shown in Fig. 4. Falcon successfully segmented designated complex targets in images based on prompts and also identified changes between two similar images.

5.2. Zero-shot Evaluation

Finally, we evaluate the capabilities of Falcon in terms of zero-shot evaluations. We present the detailed performance comparison in Tab. 8, where these evaluation datasets were not used during training. Compared with previous VLMs, Falcon achieved performance improvements over all three levels of tasks. For image-level tasks, Falcon established a new record on many datasets, such as UCM-Captions and MAR20 for image captioning and image counting. For region-level tasks and pixel-level tasks, Falcon demonstrated exceptional performance on many datasets, which required comprehensive localization and reasoning capabilities. In contrast, such capabilities were commonly missing or even not supported in prior VLMs.

5.3. Ablation experiments

This section presents the ablation studies to analyze the effects of data scale, task granularity, and model size on performance, as summarized in Tab. 9. The results demon-

strate a consistent performance improvement as the training data scale increases — for instance, from 10% training samples to 50% training samples and ultimately to 100% training samples. Furthermore, as the task granularity becomes more refined, the model not only handles more complex tasks effectively but also enhances performance on simpler ones. A comparison between the 0.3B and 0.7B parameter models reveals that a larger parameter count leads to better generalization performance. More ablation studies can be found in Sec. I of the supplementary material.

6. Conclusion

This paper develops Falcon, a holistic vision-language foundation model tailored for remote sensing with comprehensive perception and reasoning capabilities. To facilitate the training of Falcon, we further create Falcon.SFT dataset which consists of approximately 78M high-quality data samples, covering 5.6M remote sensing images. Various qualitative and quantitative experiments have demonstrated that Falcon showcased remarkable zero-shot and in-dataset performance across 14 remote sensing vision-language tasks and more than 100 test datasets. We will release the complete dataset, code, and model weights, hoping to help further advance this research field.

References

- [1] Jean-Baptiste Alayrac, Jeff Donahue, Pauline Luc, Antoine Miech, Iain Barr, Yana Hasson, Karel Lenc, Arthur Mensch, Katherine Millican, Malcolm Reynolds, et al. Flamingo: a visual language model for few-shot learning. *Advances in neural information processing systems*, 35: 23716–23736, 2022. 1
- [2] Jinze Bai, Shuai Bai, Yunfei Chu, Zeyu Cui, Kai Dang, Xiaodong Deng, Yang Fan, Wenbin Ge, Yu Han, Fei Huang, Binyuan Hui, Luo Ji, Mei Li, Junyang Lin, Runji Lin, Dayiheng Liu, Gao Liu, Chengqiang Lu, Keming Lu, Jianxin Ma, Rui Men, Xingzhang Ren, Xuancheng Ren, Chuanqi Tan, Sinan Tan, Jianhong Tu, Peng Wang, Shijie Wang, Wei Wang, Shengguang Wu, Benfeng Xu, Jin Xu, An Yang, Hao Yang, Jian Yang, Shusheng Yang, Yang Yao, Bowen Yu, Hongyi Yuan, Zheng Yuan, Jianwei Zhang, Xingxuan Zhang, Yichang Zhang, Zhenru Zhang, Chang Zhou, Jingren Zhou, Xiaohuan Zhou, and Tianhang Zhu. Qwen technical report, 2023. 6
- [3] Jinze Bai, Shuai Bai, Shusheng Yang, Shijie Wang, Sinan Tan, Peng Wang, Junyang Lin, Chang Zhou, and Jingren Zhou. Qwen-vl: A frontier large vision-language model with versatile abilities. *arXiv preprint arXiv:2308.12966*, 2023. 6, 7, 8, 28
- [4] Gerald Baier, Antonin Deschamps, Michael Schmitt, and Naoto Yokoya. Synthesizing optical and sar imagery from land cover maps and auxiliary raster data. *IEEE Transactions on Geoscience and Remote Sensing*, 60:1–12, 2021. 2
- [5] Hao Chen and Zhenwei Shi. A spatial-temporal attention-based method and a new dataset for remote sensing image change detection. *Remote Sensing*, 12(10):1662, 2020. 2
- [6] Gong Cheng, Junwei Han, Peicheng Zhou, and Lei Guo. Multi-class geospatial object detection and geographic image classification based on collection of part detectors. *ISPRS Journal of Photogrammetry and Remote Sensing*, 98: 119–132, 2014. 2
- [7] Gong Cheng, Junwei Han, and Xiaoqiang Lu. Remote sensing image scene classification: Benchmark and state of the art. *Proceedings of the IEEE*, 105:1865–1883, 2017. 2
- [8] Gong Cheng, Xiang Yuan, and Xie Junwei Han. Towards large-scale small object detection: Survey and benchmarks. *IEEE Transactions on Pattern Analysis and Machine Intelligence*, 45(11):13467–13488, 2023. 2
- [9] Qimin Cheng, Haiyan Huang, Yuan Xu, Yuzhuo Zhou, Huanying Li, and Zhongyuan Wang. Nwpu-captions dataset and mlca-net for remote sensing image captioning. *IEEE Transactions on Geoscience and Remote Sensing*, 60: 1–19, 2022. 3
- [10] Alina Ciocarlan and Andrei Stoian. Ship detection in sentinel 2 multi-spectral images with self-supervised learning. *Remote Sensing*, 13(21):4255, 2021. 2
- [11] Xavier Descombes Csaba Benedek and Josiane Zerubia. Sztaki-inria building detection benchmark. http://web.eee.sztaki.hu/remotesensing/building_benchmark.html, 2009. Accessed: 2024-11-14. 2
- [12] Wenliang Dai, Junnan Li, Dongxu Li, Anthony Tiong, Junqi Zhao, Weisheng Wang, Boyang Li, Pascale Fung, and Steven Hoi. InstructBLIP: Towards general-purpose vision-language models with instruction tuning. In *Thirty-seventh Conference on Neural Information Processing Systems*, 2023. 1
- [13] Rodrigo Caye Daudt, B. L. Saux, Alexandre Boulch, and Yann Gousseau. Multitask learning for large-scale semantic change detection. *Comput. Vis. Image Underst.*, 187, 2018. 2
- [14] Jian Ding, Nan Xue, Gui-Song Xia, Xiang Bai, Wen Yang, Michael Ying Yang, Serge Belongie, Jiebo Luo, Mihai Datcu, Marcello Pelillo, et al. Object detection in aerial images: A large-scale benchmark and challenges. *IEEE transactions on pattern analysis and machine intelligence*, 44(11):7778–7796, 2021. 2, 3, 5
- [15] Cao Quoc Dung and Youngjun Choe. Detecting damaged buildings on post-hurricane satellite imagery based on customized convolutional neural networks. *IEEE Dataport*, 2018. 2
- [16] Jeff Faudi and Martin. Airbus ship detection challenge. <https://kaggle.com/competitions/airbus-ship-detection>, 2018. Accessed: 2024-11-14. 2
- [17] Haonan Guo, Xin Su, Chen Wu, Bo Du, Liangpei Zhang, and Deren Li. Remote sensing chatgpt: Solving remote sensing tasks with chatgpt and visual models. *arXiv preprint arXiv:2401.09083*, 2024. 3
- [18] Patrick Helber, Benjamin Bischke, Andreas Dengel, and Damian Borth. Eurosat: A novel dataset and deep learning benchmark for land use and land cover classification. *IEEE Journal of Selected Topics in Applied Earth Observations and Remote Sensing*, 2017. 2
- [19] Shima Holail, Tamer Saleh, Xiongwu Xiao, and Deren Li. Afde-net: Building change detection using attention-based feature differential enhancement for satellite imagery. *IEEE Geoscience and Remote Sensing Letters*, 20:1–5, 2023. 2
- [20] Shengding Hu, Yuge Tu, Xu Han, Chaoqun He, Ganqu Cui, Xiang Long, Zhi Zheng, Yewei Fang, Yuxiang Huang, Weilin Zhao, et al. Minicpm: Unveiling the potential of small language models with scalable training strategies. *arXiv preprint arXiv:2404.06395*, 2024. 6, 7, 8, 28, 35
- [21] Yuan Hu, Jianlong Yuan, Congcong Wen, Xiaonan Lu, and Xiang Li. Rsgpt: A remote sensing vision language model and benchmark. *arXiv preprint arXiv:2307.15266*, 2023. 1, 2, 3, 32
- [22] Yuansheng Hua, Lichao Mou, Pu Jin, and Xiao Xiang Zhu. Multiscene: A large-scale dataset and benchmark for multiscene recognition in single aerial images. *IEEE Transactions on Geoscience and Remote Sensing*, 60:1–13, 2021. 2
- [23] Shunping Ji, Shiqing Wei, and Meng Lu. Fully convolutional networks for multisource building extraction from an open aerial and satellite imagery data set. *IEEE Transactions on Geoscience and Remote Sensing*, 57(1):574–586, 2019. 2
- [24] Bitao Jiang. S2looking: A satellite side-looking dataset for building change detection. *Remote Sensing*, 13, 2021. 2

- [25] Bitao Jiang. S2looking: A satellite side-looking dataset for building change detection. *Remote Sensing*, 13, 2021. 2
- [26] Serdar Kızılkaya, Ugur Alganci, and Elif Sertel. Vhrships: An extensive benchmark dataset for scalable deep learning-based ship detection applications. *ISPRS International Journal of Geo-Information*, 11(8):445, 2022. 2
- [27] Kartik Kuckreja, Muhammad Sohail Danish, Muzammal Naseer, Abhijit Das, Salman Khan, and Fahad Shahbaz Khan. Geochat: Grounded large vision-language model for remote sensing. In *Proceedings of the IEEE/CVF Conference on Computer Vision and Pattern Recognition*, pages 27831–27840, 2024. 1, 2, 3, 4, 5, 6, 7, 8, 28
- [28] Darius Lam, Richard Kuzma, Kevin McGee, Samuel Doolley, Michael Laielli, Matthew K. Klaric, Yaroslav Bulatov, and Brendan McCord. xvview: Objects in context in overhead imagery. *ArXiv*, abs/1802.07856, 2018. 2
- [29] MA Lebedev, Yu V Vizilter, OV Vygolov, Vladimir A Knyaz, and A Yu Rubis. Change detection in remote sensing images using conditional adversarial networks. *The International Archives of the Photogrammetry, Remote Sensing and Spatial Information Sciences*, 42:565–571, 2018. 2
- [30] Haifeng Li, Chao Tao, Zhixiang Wu, Jie Chen, Jianya Gong, and Min Deng. Rsi-cb: A large scale remote sensing image classification benchmark via crowdsourcing data. *ArXiv*, abs/1705.10450, 2017. 2
- [31] Haifeng Li, Hao Jiang, Xin Gu, Jian Peng, Wenbo Li, Liang Hong, and Chao Tao. Clrs: Continual learning benchmark for remote sensing image scene classification. *Sensors*, 20(4):1226, 2020. 2
- [32] Haoyang Li, Fangjie Zhu, Xiaoyu Zheng, Mengxi Liu, and Guangzhao Chen. Msdcunet: A deep learning framework for built-up area change detection integrating multispectral, sar, and vhr data. *IEEE Journal of Selected Topics in Applied Earth Observations and Remote Sensing*, 15:5163–5176, 2022. 2
- [33] Kun Li. Rs image dataset hefei. <https://aistudio.baidu.com/datasetdetail/88597>, 2021. Accessed: 2024-11-15. 2
- [34] Ke Li, Gang Wan, Gong Cheng, Liqiu Meng, and Junwei Han. Object detection in optical remote sensing images: A survey and a new benchmark. *ISPRS Journal of Photogrammetry and Remote Sensing*, 159:296–307, 2020. 3, 2
- [35] Xuyang Li, Danfeng Hong, and Jocelyn Chanussot. S2mae: A spatial-spectral pretraining foundation model for spectral remote sensing data. In *Proceedings of the IEEE/CVF Conference on Computer Vision and Pattern Recognition*, pages 24088–24097, 2024. 4
- [36] Ziyi Lin, Chris Liu, Renrui Zhang, Peng Gao, Longtian Qiu, Han Xiao, Han Qiu, Chen Lin, Wenqi Shao, and Keqin Chen. Sphinx: The joint mixing of weights, tasks, and visual embeddings for multi-modal large language models. *arXiv preprint arXiv:2311.07575*, 2023. 6, 7, 8, 28, 29
- [37] Fan Liu, DeLong Chen, Zhangqingyun Guan, Xiaocong Zhou, Jiale Zhu, Qiaolin Ye, Liyong Fu, and Jun Zhou. Remoteflip: A vision language foundation model for remote sensing. *IEEE Transactions on Geoscience and Remote Sensing*, 2024. 1, 3, 4, 6, 7
- [38] Haotian Liu, Chunyuan Li, Qingyang Wu, and Yong Jae Lee. Visual instruction tuning. *Advances in neural information processing systems*, 36, 2024. 1, 6, 8, 28
- [39] Zikun Liu, Liu Yuan, Lubin Weng, and Yiping Yang. A high resolution optical satellite image dataset for ship recognition and some new baselines. In *International conference on pattern recognition applications and methods*, pages 324–331. SciTePress, 2017. 2
- [40] Sylvain Lobry, Diego Marcos, Jesse Murray, and Devis Tuia. Rsvqa: Visual question answering for remote sensing data. *IEEE Transactions on Geoscience and Remote Sensing*, 2020. 3, 2
- [41] Yang Long, Yiping Gong, Zhifeng Xiao, and Qing Liu. Accurate object localization in remote sensing images based on convolutional neural networks. *IEEE Transactions on Geoscience and Remote Sensing*, 55:2486–2498, 2017. 2
- [42] Yang Long, Yiping Gong, Zhifeng Xiao, and Qing Liu. Accurate object localization in remote sensing images based on convolutional neural networks. *IEEE Transactions on Geoscience and Remote Sensing*, 55(5):2486–2498, 2017. 2
- [43] Yang Long, Gui-Song Xia, Shengyang Li, Wen Yang, Michael Ying Yang, Xiao Xiang Zhu, Liangpei Zhang, and Deren Li. On creating benchmark dataset for aerial image interpretation: Reviews, guidances, and million-aid. *IEEE Journal of selected topics in applied earth observations and remote sensing*, 14:4205–4230, 2021. 2, 3, 5
- [44] Xiaoqiang Lu, Binqiang Wang, Xiangtao Zheng, and Xuelong Li. Exploring models and data for remote sensing image caption generation. *IEEE Transactions on Geoscience and Remote Sensing*, 56(4):2183–2195, 2017. 3, 5, 2
- [45] Ye Lyu, George Vosselman, Gui-Song Xia, Alper Yilmaz, and Michael Ying Yang. Uavid: A semantic segmentation dataset for uav imagery. *ISPRS journal of photogrammetry and remote sensing*, 165:108–119, 2020. 3
- [46] Emmanuel Maggiori, Yuliya Tarabalka, Guillaume Charpiat, and Pierre Alliez. Can semantic labeling methods generalize to any city? the inria aerial image labeling benchmark. In *Igarss IEEE International Geoscience and Remote Sensing Symposium*, 2017.
- [47] Emmanuel Maggiori, Yuliya Tarabalka, Guillaume Charpiat, and Pierre Alliez. Can semantic labeling methods generalize to any city? the inria aerial image labeling benchmark. In *2017 IEEE International geoscience and remote sensing symposium (IGARSS)*, pages 3226–3229. IEEE, 2017. 2
- [48] Utkarsh Mall, Bharath Hariharan, and Kavita Bala. Change-aware sampling and contrastive learning for satellite images. In *Proceedings of the IEEE/CVF Conference on Computer Vision and Pattern Recognition*, pages 5261–5270, 2023. 4
- [49] Utkarsh Mall, Cheng Perng Phoo, Meilin Kelsey Liu, Carl Vondrick, Bharath Hariharan, and Kavita Bala. Remote sensing vision-language foundation models without annotations via ground remote alignment. *arXiv preprint arXiv:2312.06960*, 2023. 3

- [50] Oscar Manas, Alexandre Lacoste, Xavier Giró-i Nieto, David Vazquez, and Pau Rodriguez. Seasonal contrast: Unsupervised pre-training from uncurated remote sensing data. In *Proceedings of the IEEE/CVF International Conference on Computer Vision*, pages 9414–9423, 2021. 4
- [51] Dilxat Muhtar, Zhenshi Li, Feng Gu, Xueliang Zhang, and Pengfeng Xiao. Lhrs-bot: Empowering remote sensing with vgi-enhanced large multimodal language model. *arXiv preprint arXiv:2402.02544*, 2024. 1, 3, 4, 6, 7, 8, 28
- [52] PATREO. Aaround: Multi-view datasets. <http://patreo.dcc.ufmg.br/2020/07/22/multi-view-datasets/>, 2020. Accessed: 2024-11-15. 2
- [53] PATREO. Bh pools and water tanks datasets. <http://patreo.dcc.ufmg.br/2020/07/29/bh-pools-watertanks-datasets/>, 2020. Accessed: 2024-11-14. 2
- [54] Bo Qu, Xuelong Li, Dacheng Tao, and Xiaoqiang Lu. Deep semantic understanding of high resolution remote sensing image. In *2016 International conference on computer, information and telecommunication systems (Cits)*, pages 1–5. IEEE, 2016. 3, 2
- [55] Alec Radford, Jong Wook Kim, Chris Hallacy, Aditya Ramesh, Gabriel Goh, Sandhini Agarwal, Girish Sastry, Amanda Askell, Pamela Mishkin, Jack Clark, et al. Learning transferable visual models from natural language supervision. In *International conference on machine learning*, pages 8748–8763. PMLR, 2021. 1
- [56] Colorado J Reed, Ritwik Gupta, Shufan Li, Sarah Brockman, Christopher Funk, Brian Clipp, Kurt Keutzer, Salvatore Candido, Matt Uyttendaele, and Trevor Darrell. Scale-mae: A scale-aware masked autoencoder for multiscale geospatial representation learning. In *Proceedings of the IEEE/CVF International Conference on Computer Vision*, pages 4088–4099, 2023. 4
- [57] RSAICP. Airplane detection dataset. <https://www.rsaicp.com/portal/dataDetail?id=34>, 2020. Accessed: 2024-11-14. 2
- [58] RSAICP. Ship detection dataset. <https://www.rsaicp.com/portal/dataDetail?id=35>, 2021. Accessed: 2024-11-14. 2
- [59] Zhenfeng Shao, Ke Yang, and Weixun Zhou. Performance evaluation of single-label and multi-label remote sensing image retrieval using a dense labeling dataset. *Remote Sensing*, 10(6):964, 2018. 3, 2
- [60] Qian Shen, Jiru Huang, Min Wang, Shikang Tao, Rui Yang, and Xin Zhang. Semantic feature-constrained multitask siamese network for building change detection in high-spatial-resolution remote sensing imagery. *ISPRS Journal of Photogrammetry and Remote Sensing*, 189:78–94, 2022. 2
- [61] Jacob Shermeyer, Thomas Hossler, Adam Van Etten, Daniel Hogan, Ryan Lewis, and Daeil Kim. Rareplanes: Synthetic data takes flight. In *Proceedings of the IEEE/CVF Winter Conference on Applications of Computer Vision (WACV)*, pages 207–217, 2021. 3
- [62] Qian Shi, Mengxi Liu, Shengchen Li, Xiaoping Liu, Fei Wang, and Liangpei Zhang. A deeply supervised attention metric-based network and an open aerial image dataset for remote sensing change detection. *IEEE Transactions on Geoscience and Remote Sensing*, 60, 2022. 2
- [63] Qian Shi, Da He, Zhengyu Liu, Xiaoping Liu, and Jingqian Xue. Globe230k: A benchmark dense-pixel annotation dataset for global land cover mapping. *Journal of Remote Sensing*, 3:0078, 2023. 2
- [64] João Daniel Silva, João Magalhães, Devis Tuia, and Bruno Martins. Large language models for captioning and retrieving remote sensing images. *arXiv preprint arXiv:2402.06475*, 2024. 3
- [65] Gencer Sumbul, Marcela Charfuelan, Begüm Demir, and Volker Markl. Bigearthnet: A large-scale benchmark archive for remote sensing image understanding. In *IGARSS 2019-2019 IEEE International Geoscience and Remote Sensing Symposium*, pages 5901–5904. IEEE, 2019. 3
- [66] Xian Sun, Peijin Wang, Wanxuan Lu, Zicong Zhu, Xiaonan Lu, Qibin He, Junxi Li, Xuee Rong, Zhujun Yang, Hao Chang, et al. Ringmo: A remote sensing foundation model with masked image modeling. *IEEE Transactions on Geoscience and Remote Sensing*, 61:1–22, 2022. 4
- [67] Xian Sun, Peijin Wang, Zhiyuan Yan, Feng Xu, Ruiping Wang, Wenhui Diao, Jin Chen, Jihao Li, Yingchao Feng, and Tao Xu. Fair1m: A benchmark dataset for fine-grained object recognition in high-resolution remote sensing imagery. *ISPRS Journal of Photogrammetry and Remote Sensing*, 184, 2022. 3, 2
- [68] Yuxi Sun, Shanshan Feng, Xutao Li, Yunming Ye, Jian Kang, and Xu Huang. Visual grounding in remote sensing images. In *Proceedings of the 30th ACM International Conference on Multimedia*, page 404–412, New York, NY, USA, 2022. Association for Computing Machinery. 2
- [69] Xin-Yi Tong, Gui-Song Xia, Qikai Lu, Huanfeng Shen, Shengyang Li, Shucheng You, and Liangpei Zhang. Land-cover classification with high-resolution remote sensing images using transferable deep models. *Remote Sensing of Environment*, 237:111322, 2020. 3, 2
- [70] Xin-Yi Tong, Gui-Song Xia, Qikai Lu, Huanfeng Shen, Shengyang Li, Shucheng You, and Liangpei Zhang. Land-cover classification with high-resolution remote sensing images using transferable deep models. *Remote Sensing of Environment*, 237:111322, 2020. 2
- [71] Di Wang, Jing Zhang, Bo Du, Minqiang Xu, Lin Liu, Dacheng Tao, and Liangpei Zhang. Samrs: Scaling-up remote sensing segmentation dataset with segment anything model. *Advances in Neural Information Processing Systems*, 36, 2024. 2
- [72] Junjue Wang, Zhuo Zheng, Ailong Ma, Xiaoyan Lu, and Yanfei Zhong. Loveda: A remote sensing land-cover dataset for domain adaptive semantic segmentation. *arXiv preprint arXiv:2110.08733*, 2021. 2
- [73] Qi Wang, Shaoteng Liu, Jocelyn Chanussot, and Xuelong Li. Scene classification with recurrent attention of vhr remote sensing images. *IEEE Transactions on Geoscience and Remote Sensing*, 57(2):1155–1167, 2019. 2
- [74] Wenhai Wang, Zhe Chen, Xiaokang Chen, Jiannan Wu, Xizhou Zhu, Gang Zeng, Ping Luo, Tong Lu, Jie Zhou, Yu

- Qiao, and Jifeng Dai. Visionllm: Large language model is also an open-ended decoder for vision-centric tasks, 2023. [2](#)
- [75] Zhecheng Wang, Rajanie Prabha, Tianyuan Huang, Jiajun Wu, and Ram Rajagopal. Skyscript: A large and semantically diverse vision-language dataset for remote sensing. In *Proceedings of the AAAI Conference on Artificial Intelligence*, pages 5805–5813, 2024. [3](#), [4](#)
- [76] Syed Waqas Zamir, Aditya Arora, Akshita Gupta, Salman Khan, Guolei Sun, Fahad Shahbaz Khan, Fan Zhu, Ling Shao, Gui-Song Xia, and Xiang Bai. isaid: A large-scale dataset for instance segmentation in aerial images. In *Proceedings of the IEEE/CVF Conference on Computer Vision and Pattern Recognition Workshops*, pages 28–37, 2019. [2](#)
- [77] Jiannan Wu, Muyan Zhong, Sen Xing, Zeqiang Lai, Zhaoyang Liu, Wenhai Wang, Zhe Chen, Xizhou Zhu, Lewei Lu, Tong Lu, et al. Visionllm v2: An end-to-end generalist multimodal large language model for hundreds of vision-language tasks. *arXiv preprint arXiv:2406.08394*, 2024. [2](#), [5](#), [3](#)
- [78] Gui-Song Xia, Wen Yang, Julie Delon, Yann Gousseau, Hong Sun, and Henri Maître. Structural high-resolution satellite image indexing. In *ISPRS TC VII Symposium-100 Years ISPRS*, pages 298–303, 2010. [2](#)
- [79] Gui-Song Xia, Jingwen Hu, Fan Hu, Baoguang Shi, Xiang Bai, Yanfei Zhong, Liangpei Zhang, and Xiaoqiang Lu. Aid: A benchmark data set for performance evaluation of aerial scene classification. *IEEE Transactions on Geoscience and Remote Sensing*, 55(7):3965–3981, 2017. [2](#)
- [80] Gui-Song Xia, Xiang Bai, Jian Ding, Zhen Zhu, Serge Belongie, Jiebo Luo, Mihai Datcu, Marcello Pelillo, and Liangpei Zhang. Dota: A large-scale dataset for object detection in aerial images. In *Proceedings of the IEEE conference on computer vision and pattern recognition*, pages 3974–3983, 2018. [2](#), [3](#), [5](#)
- [81] Bin Xiao, Haiping Wu, Weijian Xu, Xiyang Dai, Houdong Hu, Yumao Lu, Michael Zeng, Ce Liu, and Lu Yuan. Florence-2: Advancing a unified representation for a variety of vision tasks. In *Proceedings of the IEEE/CVF Conference on Computer Vision and Pattern Recognition*, pages 4818–4829, 2024. [2](#), [5](#), [7](#), [8](#), [28](#), [29](#)
- [82] Qikai Lu Huangfeng Shen Shengyang Li Shucheng You Liangpei Zhang Xin-Yi Tong, Gui-Song Xia. Land-cover classification with high-resolution remote sensing images using transferable deep models. *Remote Sensing of Environment*, doi: 10.1016/j.rse.2019.111322, 2020.
- [83] Cong Yang, Zuchao Li, and Lefei Zhang. Mgimm: Multi-granularity instruction multimodal model for attribute-guided remote sensing image detailed description. *arXiv preprint arXiv:2406.04716*, 2024. [3](#)
- [84] Yi Yang and Shawn Newsam. Bag-of-visual-words and spatial extensions for land-use classification. In *Proceedings of the 18th SIGSPATIAL international conference on advances in geographic information systems*, pages 270–279, 2010. [2](#)
- [85] Wenqi Yu, Gong Cheng, Meijun Wang, Yanqing Yao, Xingxing Xie, Xiwen Yao, and Junwei Han. Mar20: A benchmark for military aircraft recognition in remote sensing images. *National Remote Sensing Bulletin*, 2023. [2](#)
- [86] Zhiqiang Yuan, Wenkai Zhang, Kun Fu, Xuan Li, Chubo Deng, Hongqi Wang, and Xian Sun. Exploring a fine-grained multiscale method for cross-modal remote sensing image retrieval. *arXiv preprint arXiv:2204.09868*, 2022. [3](#), [2](#)
- [87] Yuan Yuqian, Li Wentong, Liu Jian, Tang Dongqi, Luo Xinjie, Qin Chi, Zhang Lei, and Zhu Jianke. Osprey: Pixel understanding with visual instruction tuning, 2023. [28](#)
- [88] Yangfan Zhan, Zhitong Xiong, and Yuan Yuan. Rsvg: Exploring data and models for visual grounding on remote sensing data. *IEEE Transactions on Geoscience and Remote Sensing*, 61:1–13, 2022. [3](#), [2](#)
- [89] Yang Zhan, Zhitong Xiong, and Yuan Yuan. Skyeyegpt: Unifying remote sensing vision-language tasks via instruction tuning with large language model. *arXiv preprint arXiv:2401.09712*, 2024. [2](#), [3](#), [4](#)
- [90] Chenxiao Zhang, Peng Yue, Deodato Tapete, Liangcun Jiang, Boyi Shangguan, Li Huang, and Guangchao Liu. A deeply supervised image fusion network for change detection in high resolution bi-temporal remote sensing images. *ISPRS Journal of Photogrammetry and Remote Sensing*, 166:183–200, 2020. [2](#)
- [91] Tao Zhang, Xiangtai Li, Hao Fei, Haobo Yuan, Shengqiong Wu, Shunping Ji, Change Loy Chen, and Shuicheng Yan. Omg-llava: Bridging image-level, object-level, pixel-level reasoning and understanding. In *NeurIPS*, 2024. [2](#), [5](#), [3](#)
- [92] Wei Zhang, Miaoxin Cai, Tong Zhang, Guoqiang Lei, Yin Zhuang, and Xuerui Mao. Popeye: A unified visual-language model for multi-source ship detection from remote sensing imagery. *arXiv preprint arXiv:2403.03790*, 2024. [3](#), [4](#)
- [93] Wei Zhang, Miaoxin Cai, Tong Zhang, Yin Zhuang, and Xuerui Mao. Earthgpt: A universal multi-modal large language model for multi-sensor image comprehension in remote sensing domain. *IEEE Transactions on Geoscience and Remote Sensing*, 2024. [3](#), [4](#)
- [94] Wei Zhang, Miaoxin Cai, Tong Zhang, Yin Zhuang, and Xuerui Mao. Earthmarker: A visual prompt learning framework for region-level and point-level remote sensing imagery comprehension. *arXiv preprint arXiv:2407.13596*, 2024. [3](#)
- [95] Zhengning Zhang, Lin Zhang, Yue Wang, Pengming Feng, and Ran He. Shippersimagenet: A large-scale fine-grained dataset for ship detection in high-resolution optical remote sensing images. *IEEE Journal of Selected Topics in Applied Earth Observations and Remote Sensing*, 14:8458–8472, 2021. [2](#)
- [96] Zilun Zhang, Tiancheng Zhao, Yulong Guo, and Jianwei Yin. Rs5m and georsclip: A large scale vision-language dataset and a large vision-language model for remote sensing. *IEEE Transactions on Geoscience and Remote Sensing*, 2024. [1](#), [2](#), [3](#), [4](#)
- [97] B. Zhao, Y. Zhong, G. S. Xia, and L. Zhang. Dirichlet-derived multiple topic scene classification model for high spatial resolution remote sensing imagery. *IEEE Trans-*

- actions on Geoscience and Remote Sensing*, 54(4):2108–2123, 2016. [2](#)
- [98] Lijun Zhao, Ping Tang, and Lianzhi Huo. Feature significance-based multibag-of-visual-words model for remote sensing image scene classification. *Journal of Applied Remote Sensing*, 10, 2016. [2](#)
- [99] Weixun Zhou, Shawn Newsam, Congmin Li, and Zhenfeng Shao. Patternnet: A benchmark dataset for performance evaluation of remote sensing image retrieval. *ISPRS journal of photogrammetry and remote sensing*, 145:197–209, 2018. [2](#)
- [100] Zhuang Zhou, Shengyang Li, Wei Wu, Weilong Guo, Xuan Li, Guisong Xia, and Zifei Zhao. Nasc-tg2: Natural scene classification with tiangong-2 remotely sensed imagery. *IEEE Journal of Selected Topics in Applied Earth Observations and Remote Sensing*, 14:3228–3242, 2021. [2](#)
- [101] Deyao Zhu, Jun Chen, Xiaoqian Shen, Xiang Li, and Mohamed Elhoseiny. Minigt-4: Enhancing vision-language understanding with advanced large language models. *arXiv preprint arXiv:2304.10592*, 2023. [1](#), [6](#), [7](#), [8](#), [28](#), [29](#)
- [102] Haigang Zhu, Xiaogang Chen, Weiqun Dai, Kun Fu, Qixiang Ye, and Jianbin Jiao. Orientation robust object detection in aerial images using deep convolutional neural network. In *2015 IEEE international conference on image processing (ICIP)*, pages 3735–3739. IEEE, 2015. [2](#)
- [103] Qin Zou, Lihao Ni, Tong Zhang, and Qian Wang. Deep learning based feature selection for remote sensing scene classification. *IEEE Geoscience and Remote Sensing Letters*, 12(11):1–5, 2015. [2](#)

Falcon: A Remote Sensing Vision-Language Foundation Model

Supplementary Material

In the supplementary material, we will introduce the following content to complement the details of our study.

Contents

A. 67 collected remote sensing datasets for construction of Falcon_SFT	2
B. Unified annotation example and multi-instruction conversation example	4
C. Mapped category dictionary	6
D. Data conversion of 14 new tasks in Falcon_SFT	7
E. Qualitative comparisons of 14 tasks with state-of-the-art models	8
E.1 . Task1: Image Classification	9
E.2 . Task2: Visual Question Answering	10
E.3 . Task3: Counting Target	12
E.4 . Task4: Image Captioning	13
E.5 . Task5: Detailed Image Captioning	14
E.6 . Task6: Region Classification-HBB	18
E.7 . Task7: Region Classification-OBB	19
E.8 . Task8: Region Detection-HBB	20
E.9 . Task9: Region Detection-OBB	21
E.10. Task10: Visual Grounding	22
E.11. Task11: Region Captioning	24
E.12. Task12: Pixel Classification	25
E.13. Task13: Segmentation	26
E.14. Task14: Change Detection	27
F. Quantitative comparison results for remaining tasks	28
G. Qualitative comparisons using diversified instructions	30
H. Experiment setup for human evaluation	32
I . More ablation experiments	35
J . Evaluation metric for each task	37

A. 67 collected remote sensing datasets for construction of Falcon_SFT

Here we provide more details for the 67 collected remote sensing datasets which are used for the construction of our Falcon_SFT datasets. It should be noted that only images with annotations are considered in the construction of Falcon_SFT. Moreover, we provide the direct download link of each dataset in Table I for easy accessibility.

Dataset	Download Link	Dataset Size (Unzipped)	Number of Images Used in Our Experiments	Image Size	Image Modalities	Number of Class	Supported Tasks
AID[79]	Link	2.5GB	10000	600×600	RGB	30	Image Classification
ASD [16]	Link	30GB	42556	768×768	RGB	1	Object Detection
AiRound[52]	Link	5.9GB	1165	500×500	RGB, multi-spectral	11	Image Classification
airplane_det[57]	Link	8.8GB	430	4096×4096	RGB	1	Object Detection (Airplane)
BHP Watertanks[53]	Link	2.0GB	325	3840×2160	RGB	2	Semantic Segmentation
CDD[29]	Link	4.6GB	338	1900×1000	RGB	-	Change Detection
CLRS[31]	Link	2.8GB	15000	256×256	RGB	25	Image Classification
DIOR[34]	Link	11.7GB	23463	800×800	RGB	20	Object Detection
DIOR-RSVG[88]	Link	10.5GB	17402	800×800	RGB	20	Visual Grounding
DLRS[59]	Link	844MB	2100	256×256	RGB	17	Semantic Segmentation, Scene Classification, Image Retrieval
DOTA2.0[14]	Link	23GB	2423	800×800-20000 × 20000	RGB	18	Object Detection
DSIFN[90]	Link	531MB	7604	512×512	RGB	-	Change Detection
EGY_BCD[19]	Link	1.1GB	4366	256×256	RGB	-	Change Detection
EuroSAT[18]	Link	3.0GB	27000	64×64	RGB, multi-spectral	10	Image Classification
FAIR1M1.0[67]	Link	74GB	16488	500×500-1200×5000	RGB	36	Object Detection
GEONRW[4]	Link	30.15GB	7549	1000×1000	RGB, SAR	11	Semantic Segmentation
GID15[70]	Link	18GB	110	7200×6800	multi-spectral	15	Semantic Segmentation
Globe230k[63]	Link	12GB	232819	512×512	RGB	10	Semantic Segmentation
Hefe[33]	Link	11MB	533	256×256	RGB	5	Image Classification
RSVQA HR[40]	Link	14GB	9505	512×512	RGB	89	VQA
HRSC2016[39]	Link	7.0GB	1070	1000×600	RGB	1	Object Detection
HRSCD[13]	Link	12GB	554	10000×10000	RGB	2/6	Change Detection, Land Cover Classification
Hurricane_Damage[15]	Link	71MB	23000	128×128	RGB	2	Image Classification
Inria[47]	Link	26GB	180	5000×5000	RGB	2	Semantic Segmentation
ISAID[76]	Link	20.9GB	1869	500×500-1200×5000	RGB	15	Instance Segmentation
LEVIR-CD[5]	Link	2.4GB	1098	1024×1024	RGB	-	Change Detection
LEVIR-CD+[24]	Link	7.1GB	1766	1024×1024	RGB	-	Change Detection
LoveDA[72]	Link	9.0GB	4191	1024×1024	RGB	8	Semantic Segmentation
RSVQA LR[40]	Link	199MB	772	256×256	RGB	89	VQA
MAR20[85]	Link	2.3GB	3842	800×800	RGB	20	Object Detection
million-AID[43]	Link	136G	10000	256 × 256, 512 × 512	RGB	51	Image Classification
MSBC[32]	Link	3.2GB	7402	256×256	multi-spectral	2	Change Detection
MSOSCD[32]	Link	2.4GB	10144	256×256	multi-spectral	2	Change Detection
MultiScene[22]	Link	7.6GB	100000	512×512	RGB	36	Multilable Image Classification
NaSC_TG2[100]	Link	8.8GB	20000	128×128	multi-spectral	10	Image Classification
NJDS[60]	Link	1.2GB	2	14231×11381	RGB	-	Change Detection, Semantic Segmentation
NWPU_RESISC45[7]	Link	414MB	31500	256×256	RGB	45	Image Classification
NWPU-VHR-10[6]	Link	74MB	650	900×500	RGB, Infrared	10	Image Classification, Object Detection
OPTIMAL31[73]	Link	25MB	1860	256×256	RGB	31	Image Classification
PatternNet[99]	Link	1.4GB	30400	256×256	RGB	38	Image Classification
RS_C1[98]	Link	925MB	1232	512×512	RGB	11	Image Classification
RSD46_WHU[41]	Link	9.7GB	100131	256×256	RGB	4	Image Classification
RSL_CBJ[30]	Link	6.3GB	61454	256 × 256, 128 × 128	multi-spectral	35	Image Classification
RSICap[21]	Link	1.3GB	2685	512×512	RGB	16	Image Caption
RSICD[44]	Link	1.1GB	10734	224×224	RGB	30	Image Caption
RSITMD[86]	Link	911MB	4743	256×256	RGB	32	Image Caption, Image Classification
RSOD[42]	Link	318MB	936	227×227	RGB	4	Object Detection
RSSCN7[103]	Link	352MB	2800	400×400	RGB	7	Image Classification
RSVG[68]	Link	1.5GB	4239	1024×1024	RGB	10	Object Retrieval
S2Looking[25]	Link	14GB	1970	1024×1024	multi-spectral	-	Change Detection
S2-SHIPS[10]	Link	5.2GB	16	1783×938	multi-spectral	1	Object Detection (Ship)
SAMRS[71]	Link	99.2GB	93352	600×600-1024×1024	RGB	18, 20, 37	Semantic Segmentation
ship_det[58]	Link	2.6GB	25	20000×20000	SAR	1	Object Detection (Ship)
ShipRSImagerNet[95]	Link	8.4GB	2748	930×930	RGB	50	Object Detection (Ship)
SIRL_WHU[97]	Link	1.1GB	2400	200×200	high resolution	12	Image Classification
SODA-A[8]	Link	12GB	2513	4800 × 2700	RGB	9	Object Detection
Sydney_Captions[54]	Link	441MB	530	500×500	RGB	-	Image Caption
SYSU-CD[62]	Link	11GB	40000	256×256	RGB	3	Change Detection
SZTAKI[11]	Link	4.6MB	9	930×930	RGB	2	Object Detection
UCAS-AOD[102]	Link	3.3GB	1510	1280×659	RGB	3	Object Detection
UCM-Captions[54]	Link	819MB	2100	256×256	RGB	21	Image Caption
UCM-Classification[84]	Link	819MB	2100	256×256	RGB	21	Image Classification
VHRShips[26]	Link	3.4GB	5275	2272×1270,1280×720	RGB	34	Object Detection
WHU_GID[69]	Link	6.1G	30000	112×112, 56×56	multi-spectral	15	Semantic Segmentation
WHU-CD[23]	Link	2.1GB	3900	512×512	RGB	-	Change Detection
WHU_RS19[78]	Link	114M	1005	600×600	RGB	19	Image Classification
xView[28]	Link	24G	846	2500×2500-3200×5000	RGB	60	Object Detection

Table I. 67 collected remote sensing datasets for the construction of Falcon_SFT.

Integrating Remote Sensing Datasets. After finishing dataset collections, we further integrate the 67 collected remote sensing datasets, a process that presents several challenges, including:

- *Inconsistent Annotation Formats.* There are differences in annotation formats across various datasets. For example, different datasets may follow distinct annotation standards or conventions for segmentation masks, such as polygons or mask images, making data integration and unified processing more complex. To address this, we propose to establish a unified annotation standard and convert all datasets to this format. Automated scripts are developed to transform different data formats into the

Spatial hierarchy	Tasks	#images	#Annotations
Image Level	Cls	1.35M	9.43M
	Cap	24.7K	343.5K
	D.Cap	15.9K	89.6K
	Count	316.2K	5.67M
	VQA	17.2K	4.36M
Region Level	Cls ^{hbb}	121K	3.15M
	Cls ^{obb}	241.5K	6.26M
	R.Cap	15.3K	231.2K
	Det ^{hbb}	885.3K	10.78M
	Det ^{obb}	1.01M	11.97M
	VG	15.3K	231.2K
Pixel Level	Cls ^{poly}	764.3K	15.87M
	Seg	764.3K	9.31M
	CD	76.5K	528.8K

Table II. Image and annotation statistics of the Falcon_SFT dataset.

specified standard, reducing the complexity of data integration and ensuring consistent processing. Please see Section B of the supplementary material for examples of the unified annotation format in our proposed Falcon_SFT dataset.

- *Inconsistent Category Naming.* There are inconsistencies in category naming, namely, the same target objects are labeled with different category names across different datasets. For example, “car” is labeled as “car” in some datasets [59] and as “vehicle” in others [34], leading to inconsistencies in category labeling. To solve this issue, we propose to create a unified category naming dictionary to map different labels for the same objects to a standardized category name. This can be achieved through a combination of automated mapping rules and manual interventions, ensuring consistent category naming across datasets. Please see Section C of the supplementary material for the unified category naming dictionary.

Data Repurposing and Task Expansion. The collected raw datasets cover 7 tasks, including image classification, object detection, image segmentation, image caption, visual question answering, visual grounding, and change detection. To further extend the application scenarios of our dataset, we propose to repurpose existing data structure to generate more annotations for additional tasks, enabling support for 14 tasks in total. Please see Section D of the supplementary material for the data conversion of 14 new tasks in our proposed Falcon_SFT. Specifically, we divide 14 tasks into image-level, region-level and pixel-level. At the image level, tasks involve Image Classification, Image VQA, Counting, Image Captioning and Image Detailed Captioning. At the region level, tasks involve Region Classification-HBB, Region Classification-OBB, Region Detection-HBB, Region Detection-OBB, Visual Grounding and Region Captioning. At the pixel level, tasks involve Pixel Classification, Pixel Segmentation, Change Detection. This division was also discussed in [77, 91].

B. Unified annotation example and multi-instruction conversation example

Example 1 Unified annotation format in Falcon_SFT

```
{
  "info": {
    "dataset": "",
    "modality": "[RGB-Satellite/RGB-Aerial]",
    "task": "[Classification/Caption/Detection/Segmentation/Region Caption/
    Visual Grounding/VQA/Retrieval/Change Detection]",
    "categories": ["", "", ""]
  },
  "data": [
    {
      "image": ["[Image address 1]", "[Image address 2]"]
      "size": ["width", "height"]

      "image_annotations": {
        "image_label": ["[Image-level classification]"],
        "short_description": "[Image-level short description]",
        "detailed_description": "[Image-level detailed description]",
      }

      "object_annotations": [
        {
          "bbox": [],
          "bbox_type": "[obb/hbb]"
          "label": "[Category]",
          "description": "[Description of object]"
          "segmentation": [],
          "segmentation_mask": "[path/to/mask]",
        },
        {
          "bbox": [],
          "bbox_type": "[obb/hbb]"
          "label": "[Category]",
          "description": "[Description of object]"
          "segmentation": [],
          "segmentation_mask": "[path/to/mask]",
        },
        {
          ...
        }
      ]
    },
    {
      ...
    }
  ]
}
```

Example 2 Multi-instruction conversation example in Falcon_SFT.

```
[
{
  "id": "000002227258",
  "images": ["AID/Parking/parking_311.jpg"],
  "modality": "RGB-Satellite",
  "crop": [],
  "conversations": [
    {
      "role": "user",
      "content": "<image>\n[IMG_CLS]\nAllocate a category to the image.
Classes: railway station, farmland, storage tank, park, mountain,
playground, bare land, forest, pond, church, stadium, grassland,
building, desert, resort, parking lot, baseball field, school,
airport, river, square, beach, viaduct, commercial area,
residential area, industrial area, harbor, bridge.
\nUse one or a few words."
    },
    {
      "role": "assistant",
      "content": "parking lot."
    }
  ]
},
{
  "id": "000002227259",
  "images": ["AID/Parking/parking_311.jpg"],
  "modality": "RGB-Satellite",
  "crop": [],
  "conversations": [
    {
      "role": "user",
      "content": "<image>\n[IMG_CLS]\nClassify the image.
Classes: railway station, farmland, storage tank, park, mountain,
playground, bare land, forest, pond, church, stadium, grassland,
building, desert, resort, baseball field, school, airport, river,
square, beach, viaduct, commercial area, residential area,
industrial area, harbor, bridge. \nAnswer in brief."
    },
    {
      "role": "assistant",
      "content": "The image does not belong to any of the candidate categories
you specified."
    }
  ]
},
{
  ...
}
```

C. Mapped category dictionary

Num.	Category	Num.	Category	Num.	Category	Num.	Category
1	agriculture area	2	aircraft hangar	3	airplane	4	airport
5	airport runway	6	apron	7	aquaculture	8	avenue
9	bare land	10	baseball field	11	basketball court	12	beach
13	bridge	14	building	15	cement mixer	16	cemetery
17	chimney	18	church	19	cloud	20	coastline
21	commercial area	22	construction site	23	container	24	crane
25	crosswalk	26	dam	27	damaged building	28	desert
29	excavator	30	expressway service area	31	expressway toll station	32	factory area
33	farmland	34	field	35	football field	36	footbridge
37	forest	38	fork road	39	freeway	40	garden
41	golf field	42	graff	43	grassland	44	green house
45	greenbelt	46	ground track field	47	harbor	48	helicopter
49	helipad	50	highway	51	hirst	52	ice
53	ice land	54	impervious surface	55	industrial area	56	intersection
57	irrigated area	58	island	59	lake	60	lakeshore
61	locomotive	62	mine	63	mountain	64	oil gas field
65	oil well	66	orchard	67	overpass	68	palace
69	park	70	parking lot	71	pasture	72	pavement
73	pipeline	74	playground	75	pond	76	power station
77	pylon	78	quarry	79	railway	80	railway station
81	refinery	82	residential area	83	resort	84	river
85	road	86	rock land	87	roundabout	88	runway
89	rural residential area	90	school	91	sea	92	sewage
93	shed	94	ship	95	shipping yard	96	shrub land
97	snowberg	98	soccer ball field	99	solar panel	100	solar power station
101	square	102	stadium	83	statue	84	steelsmelter
105	storage land	106	storage tank	107	stream	108	substation
109	swimming pool	110	tennis court	111	tent	112	terrace
113	terraced field	114	thermal power station	115	tower	116	town
117	train carriage	118	transformer station	119	tree	120	tundra
121	turning circle	122	urban residential area	123	vehicle	124	viaduct
125	wastewater plant	126	water area	127	wetland	128	wind turbine
129	windmill						

Table III. Mapped object category exploited in Falcon_SFT.

D. Data conversion of 14 new tasks in Falcon_SFT

Raw Task	New Task	Explanation
Image Classification	Image Classification	Set the category of the image as the answer.
VQA	VQA	No changes.
Image Caption	Image Caption	Set a description with less than 4 sentences / 35 words as the answer.
Image Caption	Detailed Image Caption	Set a description with more than or equal to 4 sentences / 35 words as the answer.
Visual Grounding	Visual Grounding	Set a description as the question, and the corresponding bounding box as the answer.
Visual Grounding	Region Caption	Set a bounding box as the question, and the corresponding description as the answer.
Object Detection-OBB&HBB	Image Classification	Set the category of all objects contained in the image as the answer.
Object Detection-OBB&HBB	Counting Target	Set a category as the question and the total number of the corresponding boxes as the answer.
Object Detection-OBB	Region Classification-OBB	Set a bounding box as the question, and set the corresponding category as the answer.
Object Detection-OBB	Region Detection-OBB	Set a category as the question and set all the corresponding bounding boxes as the answer.
Object Detection-HBB	Region Classification-HBB	Set a bounding box as the question, and set the corresponding category as the answer.
Object Detection-HBB	Region Detection-HBB	Set a category as the question, and set all the corresponding bounding boxes as the answer.
Semantic Segmentation	Image Classification	Set the category of all objects contained in the image as the answer.
Semantic Segmentation	Pixel Classification	Set a polygon as the question, and set the corresponding category as the answer.
Semantic Segmentation	Semantic Segmentation	Set a category as the question, and set all the corresponding polygons as the answer
Semantic Segmentation	Region Detection-OBB	Replace the polygons with its horizontal enclosing rectangles as the answer.
Semantic Segmentation	Region Detection-HBB	Replace the polygons with its minimum enclosing rectangles as the answer
Change Detection	Change Detection	Set the changing polygon area as the answer.

Table IV. We convert 7 raw tasks to 14 new tasks for the construction of Falcon_SFT. 7 raw tasks are: Image Classification, VQA, Image Caption, Visual Grounding, Object Detection, Semantic Segmentation and Change Detection. 14 new tasks are: Image Classification, VQA, Image Caption, Detailed Image Caption, Visual Grounding, Region Caption, Counting Target, Region Classification-OBB, Region Detection-OBB, Region Classification-HBB, Region Detection-HBB, Pixel Classification, Semantic Segmentation and Change Detection.

E. Qualitative comparisons of 14 tasks with state-of-the-art models

In this section, we visualized the prediction results for each task and conducted a qualitative comparison between Falcon and other advanced remote sensing VLMs. The results highlight the strength and efficiency of Falcon.

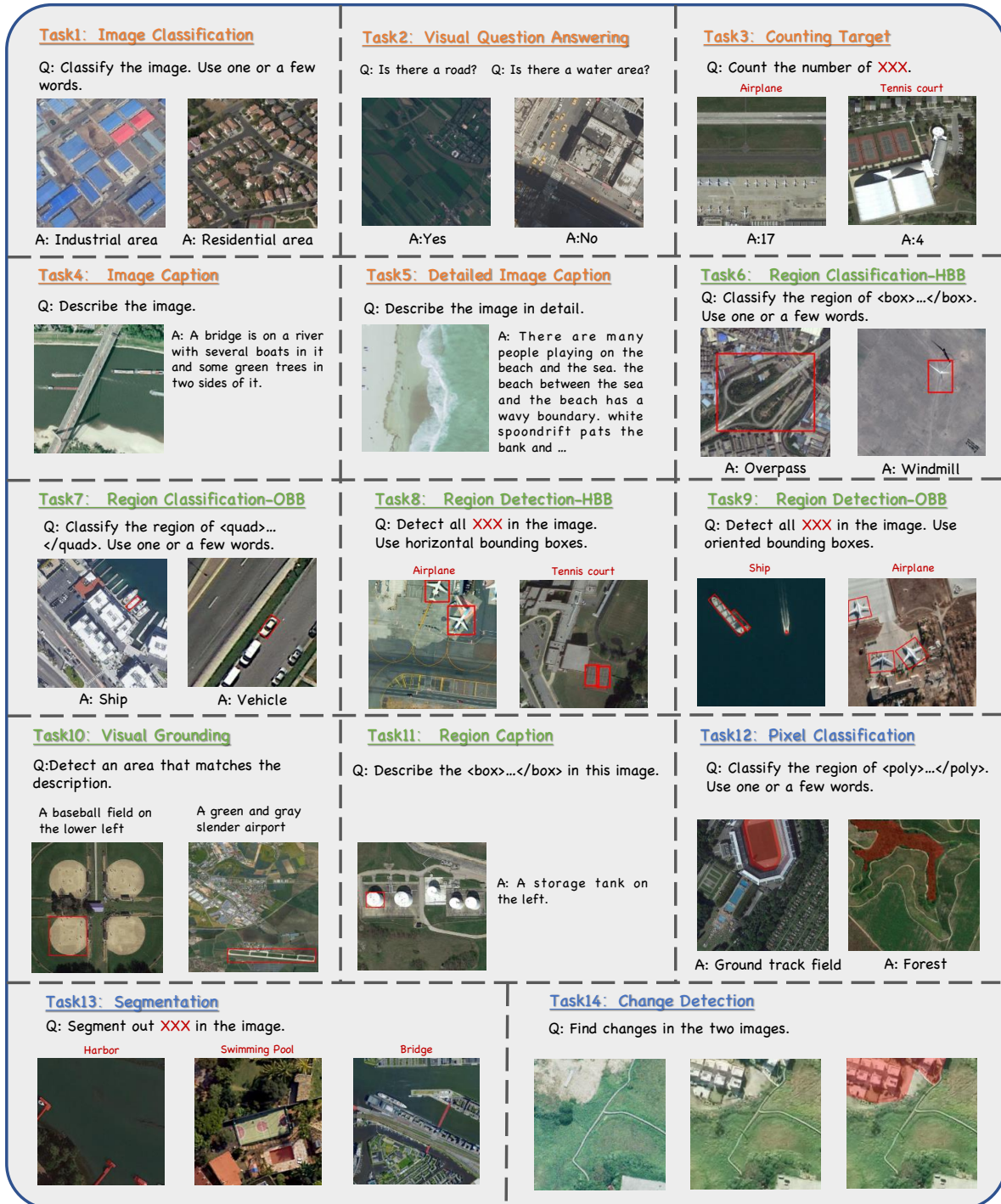


Figure I. Overview on the qualitative results of Falcon in 14 tasks.

E.1. Task1: Image Classification

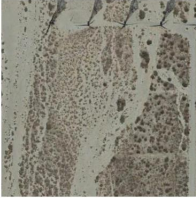
Image Classification					
					
Ground Truth	park	windmill	building, road, grassland, residential area	oil gas field, river, farmland, forest	playground
Falcon (Ours)	park	windmill	building, road, residential area	oil gas field, forest.	playground
LHRS-Bot	Landscape	Desert	residential area	Industrial area	Sports field
Geochat	baseball-field	helicopter	residential area	expressway-service-area	football-field
LLaVa-v1.5	building	desert	residential area	forest	soccer ball field
MiniGPT-v2	the campus	the area	the image	the area	the soccer field
sphinx	Aerial	Aerial	Residential area	Aerial	Aerial
MiniCPM	Aerial view of urban infrastructure.	Aerial photograph of vegetation.	road	Aerial View of Industrial Facility	Aerial View of a Soccer Field
Qwen-chat	Aerial view of a large campus with buildings and roads.	Desert	Residential area	Aerial view of a drilling site	Aerial view of a soccer field
Remote CLIP	bridge	helicopter, airplane	road	quarry	playground

Figure II. Qualitative comparisons in the task of image classification.

E.2. Task2: Visual Question Answering

Visual Question Answering

 <p>Q: Are there less residential buildings than roads in the image? (Ground truth: No.)</p>	 <p>Q: Are there less buildings than water areas in the image? (Ground truth: No.)</p>
<p>Falcon: no. ✔</p>	<p>Falcon: no. ✔</p>
<p>LHRS-Bot: No ✔</p>	<p>LHRS-Bot: No ✔</p>
<p>Geochat: No, there are not less residential buildings than roads in the image. ✔</p>	<p>Geochat: No, there are no buildings in the image. ✔</p>
<p>LLaVA-1.5: Yes, there are more roads than residential buildings in the image. ✘</p>	<p>LLaVA-1.5: Yes, there are fewer buildings in the image than water areas. ✘</p>
<p>MiniGPTv2: yes ✘</p>	<p>MiniGPTv2: yes ✘</p>
<p>Sphinx: yes ✘</p>	<p>Sphinx: yes ✘</p>
<p>Florence-2-L: yes ✘</p>	<p>Florence-2-L: yes ✘</p>
<p>MiniCPM-V: yes ✘</p>	<p>MiniCPM-V: No. ✔</p>
<p>Qwen-VL-Chat: no ✔</p>	<p>Qwen-VL-Chat: no ✔</p>

Figure III. Qualitative comparisons in the task of VQA.

Visual Question Answering



Q: Are there less residential buildings than forests? (Ground truth: No.)

Falcon: no. ✓

LHRS-Bot: No ✓

Geochat: No ✓

LLaVA-1.5: Yes, there are fewer residential buildings in the image compared to the number of trees. The image shows a city street with a few buildings, but ✗

MiniGPTv2: yes ✗

Sphinx: Yes, there are more forests than residential buildings in the image. ✗

Florence-2-L: no ✓

MiniCPM-V: No. ✓

Qwen-VL-Chat: no ✓



Q: Is there a building at the top of a road? (Ground truth: No.)

Falcon: no. ✓

LHRS-Bot: Yes ✗

Geochat: Yes ✗

LLaVA-1.5: No, there is no building at the top of a road. The image shows a parking lot with cars parked in it. ✓

MiniGPTv2: no ✓

Sphinx: no ✓

Florence-2-L: no ✓

MiniCPM-V: no ✓

Qwen-VL-Chat: no ✓

Figure IV. Qualitative comparisons in the task of VQA.

E.3. Task3: Counting Target

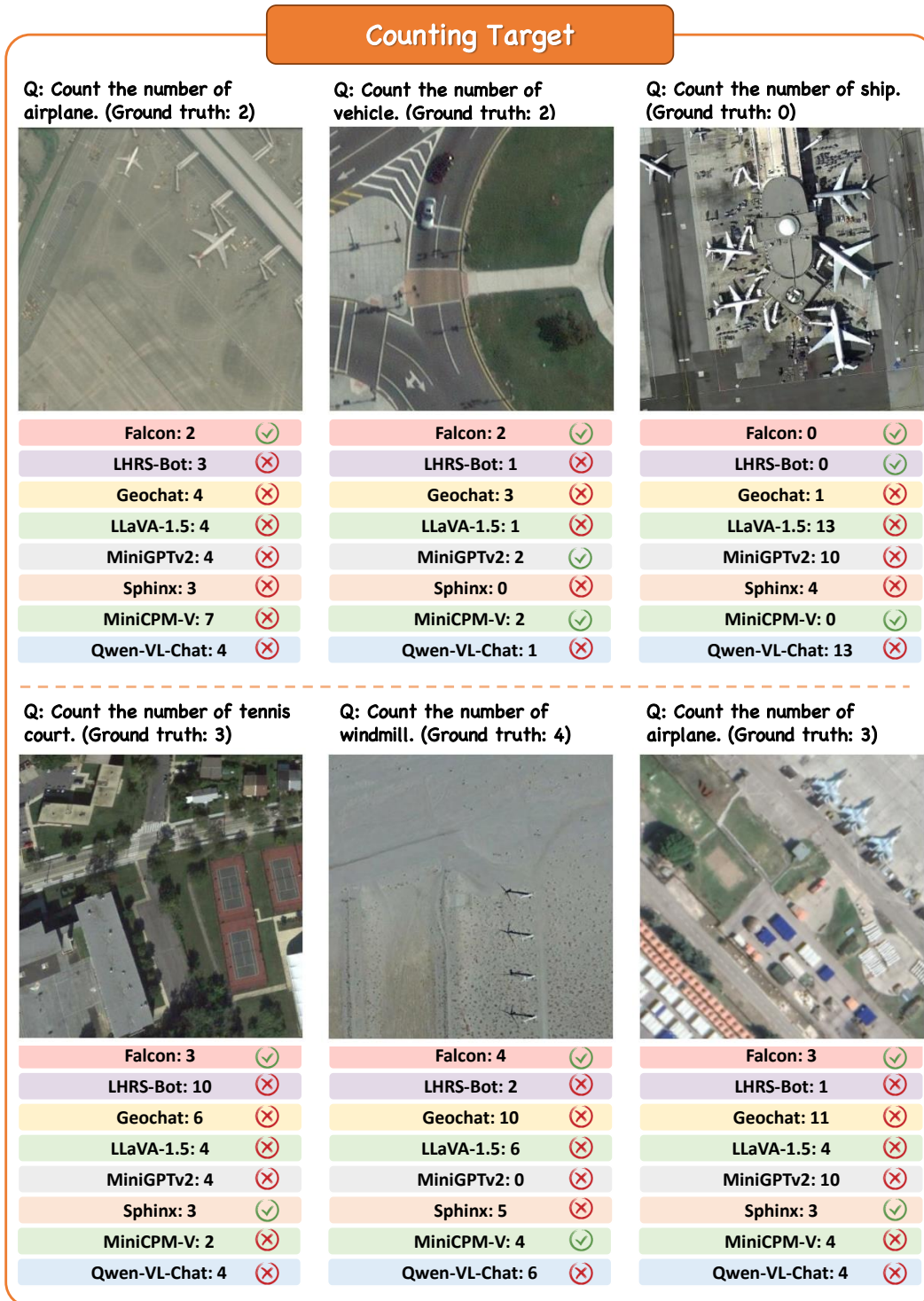


Figure V. Qualitative comparisons in the task of counting.

E.4. Task4: Image Captioning

Image Caption				
				
Ground Truth	Many houses arranged neatly with a piece of lawn beside.	A meadow with scattered bushes and some bunkers on it.	Two huge cylindrical buildings occupy most of them. A big green plants in the picture.	This is an aerial image showing an airport. There is a white airplane parked on a greyish empty space.
Falcon	A residential area with houses arranged neatly and divided into rectangles by some roads.	A meadow with some green bushes and white bunkers on it while a highway beside.	Two white storage tanks are close to several buildings and some green trees.	This is an aerial image showing an airport. There is a white airplane parked on the tarmac.
LHRS-Bot	Residential area	Golf course	Residential area	Aerial view of an airport
GeoChat	There are <p>some buildings</p> {<11><45><23><53><11>}<delim>{<0><26><10><34><90>} located close to each other at the left side of the scene.	In the satellite image, there is <p>a golf field </p> {<20> <0> <84> <80> <90>} located near some trees in the image.	There are <p>some buildings</p> {<59><76><75><88><89>}<delim>{<64><89><72><100><90>} located close to each other at the bottom of the scene.	There are <p> two white large airplanes </p> {<0><6><42><42><25>}<delim>{<0><2><10><10><90>} positioned close to each other at the top left corner.
LlaVa_v1.5	The image is an aerial view of a residential neighborhood with a mix of houses and apartments.	A golf course showcasing the layout of the course and the surrounding landscape.	The image features a large, grassy field with two large white tanks or domes in the middle of it.	The image features a large white airplane parked on a runway, with its nose close to the grass.
MiniGPT-v2	A neighborhood from above with many houses.	A golf course with many trees and a few golfers.	A large field with two large tanks in the middle.	A plane is parked on the runway of an airport.
Sphinx	The image is an aerial view of a neighborhood, showcasing a variety of houses and trees.	The image provided is a golf course. From this perspective, one can observe the layout of the fairways, and roughs.	The image is an aerial view of a parking lot with a large white building in the background.	The image is an aerial view of a large airplane parked on a runway. The airplane is positioned towards the left side of the scene.
Florence-2-L	An aerial view of a city with lots of buildings.	An aerial view of a golf course.	An aerial view of a field with two large buildings.	An airplane is shown from above on a runway.
MiniCPM-V	The image is an aerial view of a suburban neighborhood.	Aerial photograph of vegetation.	An industrial facility. The two large, white structures in the center are likely storage tanks.	The image provided is an aerial view of an aircraft parked on the tarmac. It is a commercial jet.
Qwen-VL-Chat	An aerial view of a residential area.	A satellite view of a golf course.	An aerial view of the facility.	This is a photo of a plane taken from the air.

Figure VI. Qualitative comparisons in the task of image captioning. The hallucinations of other VLMs are highlighted in red.

E.5. Task5: Detailed Image Captioning

Detailed Image Caption



This satellite image mainly shows farmland and residential areas in rural areas. The farmland is divided into multiple rectangular plots, showing different colors of green, which may be due to the difference in crop type or growth stage. These farmland is tightly arranged to form a grid-like pattern. The residential area is composed of densely arranged houses, and the roof color is different, mainly red and gray. In addition, there are some roads interspersed between farmland, connecting various villages and farmland. There are a large number of farmland in the picture, which are distributed in rectangular, with different colors. There is a dense residential area in the lower left corner of the image, composed of many red roof houses.

Figure VII. Qualitative results in the task of detailed image captioning from Falcon. Some key correct information is highlighted in green.

Detailed Image Caption



Geochat:

The image depicts a cityscape with a mix of buildings and greenery. There are two buildings close to each other at the bottom left, and another building is located at the bottom right. In the center of the image, there are two buildings and some trees, creating a focal point in the scene. The presence of trees and buildings of different sizes and shapes adds a sense of depth and complexity to the image.

Florence-2-L

This is an aerial view. In this image we can see buildings, trees, fields and roads.

Qwen-VL-Chat

A satellite image shows a town in the bottom left corner and a farm in the top right corner. The town is filled with many small, colorful houses. Just above the town, the farm has several large, colorless rectangular shapes. These are likely the foundations of structures, possibly for more houses or other buildings.

Figure VIII. Qualitative results in the task of detailed image captioning from other VLMs. In comparison, Falcon provided more detailed and accurate information.

Detailed Image Caption



Florence-2-L

This is an aerial view. In this image we can see buildings, roads, water, trees and ground.

Geochat:

The image depicts a river scene with **two bridges**, one **at the bottom** and another **at the top right**. There are **two buildings** close to each other at the bottom right, and another building at the top left. Additionally, there are **two buildings** at the top right, and one building at the top left. There are **two roads**, one **at the bottom** and another **at the top right**. There are **two dams**, one at the bottom and another at the top right. There are **two soccer fields**, one at the bottom right and another at the top right. There are **two tennis courts**, one at the bottom right and another at the top right. **There are two buildings at the top left, and one building at the top right.** **There are two roads at the top right, and one road at the bottom.** **There are two dams at the bottom and another at the top right.** **There are two soccer fields at the bottom right and another at the top right.** **There are two tennis courts at the bottom right and another at the top right.** **There are two buildings at the top left, and one building at the top right.** **There are two roads at the top right, and one road at the bottom.** **There are two dams at the bottom.**

Figure IX. Qualitative results in the task of detailed image captioning from other VLMs. The hallucinations of other VLMs are highlighted in red and some repetitive sentences are marked in blue. In comparison, Falcon provided more detailed and accurate information.

Detailed Image Caption



This satellite image captures a vast farmland and residential area, as well as a wide river. The farmland is divided into multiple small pieces, which may be to facilitate management and farming. The colors of these farmland are different, suggesting the existence of different crops or the impact of seasonal changes. The residential area is composed of densely arranged houses, surrounded by farmland and green space. The river flows through the center of the image, and its two sides of the strait are surrounded by dense forests. There are a large number of farmland in the picture, which are divided into many small pieces and may be used for planting crops. There is a wide rivers in the center, and there are dense forests on both sides. The residential area in the image consists of dense houses, and the roof color is mainly red and gray.

Figure X. Qualitative results in the task of detailed image captioning from Falcon. Some key correct information is highlighted in green.

E.6. Task6: Region Classification-HBB

Region Classification-HBB



Ground Truth: Airplane

Q: Classify the region of `<box><797><191><1000><496></box>`.
Use one or a few words.
Falcon: airplane. ✔

Q: [identify] this `{<80><19><100><50>}` is
MiniGPTv2: plane on right ✔

Q: Classify the region of `[797,191,1000,496]`.
Use one or a few words.
Sphinx: Runway. ✘

Q: `<REGION_TO_CATEGORY><loc_797><loc_191><loc_1000><loc_496>`
Florence-2-L: airplane ✔



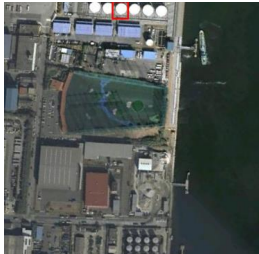
Ground Truth: Bridge

Q: Classify the region of `<box><348><415><763><699></box>`.
Use one or a few words.
Falcon: bridge. ✔

Q: [identify] this `{<35><42><76><70>}` is
MiniGPTv2: the bridge ✔

Q: Classify the region of `[348,415,763,699]`.
Use one or a few words.
Sphinx: Water. ✘

Q: `<REGION_TO_CATEGORY><loc_348><loc_415><loc_763><loc_699>`
Florence-2-L: train ✘



Ground Truth: Storage tank

Q: Classify the region of `<box><422><0><484><67></box>`.
Use one or a few words.
Falcon: storage tank. ✔

Q: [identify] this `{<42><0><48><7>}` is
MiniGPTv2: the water tanks ✘

Q: Classify the region of `[422,0,484,67]`.
Use one or a few words.
Sphinx: Water ✘

Q: `<REGION_TO_CATEGORY><loc_422><loc_0><loc_484><loc_67>`
Florence-2-L: window ✘

Figure XI. Qualitative comparisons in the task of region classification-HBB. The red bounding box in each image is for visualization only.

E.7. Task7: Region Classification-OBB

Region Classification-OBB

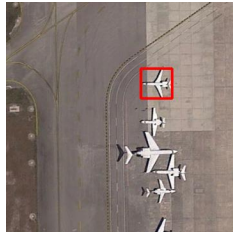
Falcon	<p>Q: Classify the region of $\langle \text{quad} \langle 392 \rangle \langle 446 \rangle \langle 324 \rangle \langle 386 \rangle \langle 292 \rangle \langle 423 \rangle \langle 359 \rangle \langle 483 \rangle \langle / \text{quad} \rangle$. Use one or a few words.</p>  <p style="text-align: center;">Swimming pool</p>	<p>Q: Classify the region of $\langle \text{quad} \langle 868 \rangle \langle 763 \rangle \langle 884 \rangle \langle 728 \rangle \langle 821 \rangle \langle 699 \rangle \langle 806 \rangle \langle 732 \rangle \langle / \text{quad} \rangle$. Use one or a few words.</p>  <p style="text-align: center;">Ship</p>	<p>Q: Classify the region of $\langle \text{quad} \langle 496 \rangle \langle 554 \rangle \langle 462 \rangle \langle 489 \rangle \langle 435 \rangle \langle 502 \rangle \langle 469 \rangle \langle 567 \rangle \langle / \text{quad} \rangle$. Use one or a few words.</p>  <p style="text-align: center;">Vehicle</p>	<p>Q: Classify the region of $\langle \text{quad} \langle 107 \rangle \langle 147 \rangle \langle 152 \rangle \langle 199 \rangle \langle 387 \rangle \langle 0 \rangle \langle 282 \rangle \langle 0 \rangle \langle / \text{quad} \rangle$. Use one or a few words.</p>  <p style="text-align: center;">Bridge</p>
	<p>Q: Classify the region of $\langle \text{quad} \langle 284 \rangle \langle 133 \rangle \langle 284 \rangle \langle 59 \rangle \langle 203 \rangle \langle 59 \rangle \langle 203 \rangle \langle 133 \rangle \langle / \text{quad} \rangle$. Use one or a few words.</p>  <p style="text-align: center;">Windmill</p>	<p>Q: Classify the region of $\langle \text{quad} \langle 724 \rangle \langle 992 \rangle \langle 724 \rangle \langle 951 \rangle \langle 680 \rangle \langle 951 \rangle \langle 680 \rangle \langle 992 \rangle \langle / \text{quad} \rangle$. Use one or a few words.</p>  <p style="text-align: center;">Storage tank</p>	<p>Q: Classify the region of $\langle \text{quad} \langle 703 \rangle \langle 420 \rangle \langle 703 \rangle \langle 292 \rangle \langle 571 \rangle \langle 292 \rangle \langle 571 \rangle \langle 420 \rangle \langle / \text{quad} \rangle$. Use one or a few words.</p>  <p style="text-align: center;">Airplane</p>	<p>Q: Classify the region of $\langle \text{quad} \langle 580 \rangle \langle 933 \rangle \langle 580 \rangle \langle 871 \rangle \langle 460 \rangle \langle 871 \rangle \langle 460 \rangle \langle 933 \rangle \langle / \text{quad} \rangle$. Use one or a few words.</p>  <p style="text-align: center;">Tennis court</p>

Figure XII. Qualitative results in the task of region classification-OBB. The red bounding box in each image is for visualization only.

E.8. Task8: Region Detection-HBB

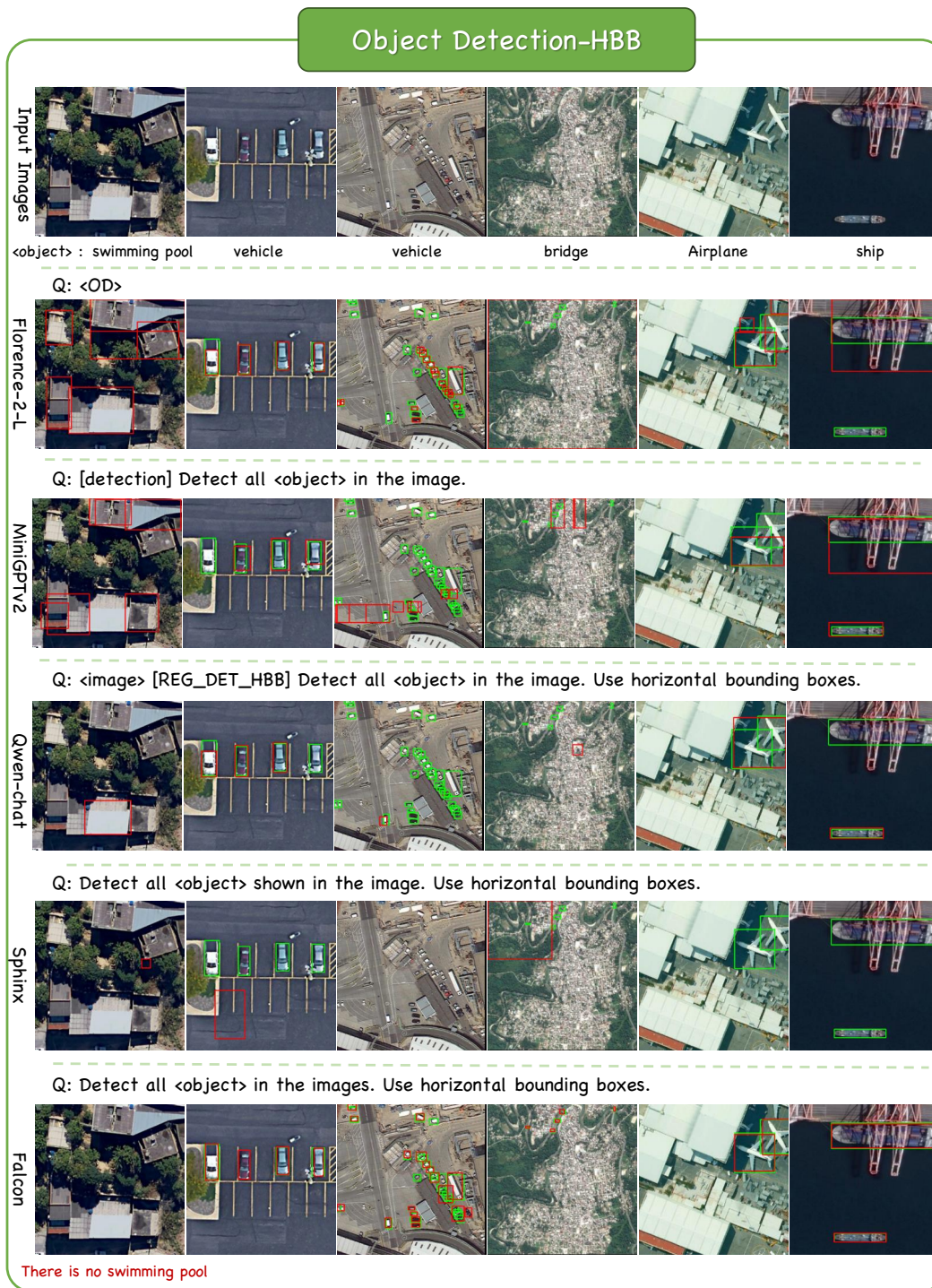


Figure XIII. Qualitative comparisons in the task of region detection-HBB. The red bounding boxes are the prediction results, while the green bounding boxes are the ground truth. Falcon successfully detected objects with tiny sizes.

E.9. Task9: Region Detection-OBB

Region Detection-OBB

Q: Detect all <object> in the images. Use oriented bounding boxes.

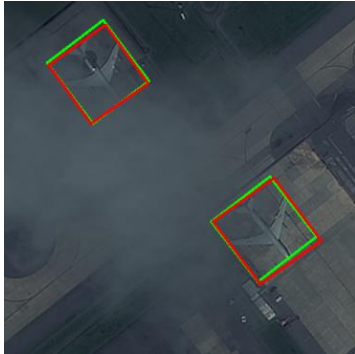
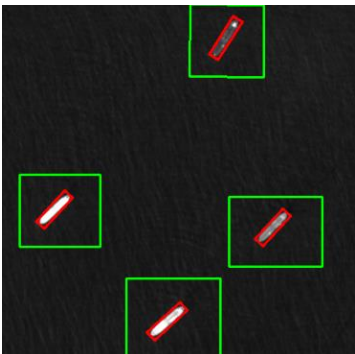
	
<object> : airplane	<object> : vehicle
	
<object> : ship	<object> : ship
	
<object> : ship	<object> : ship

Figure XIV. Qualitative results in the task of region detection-OBB. The red bounding boxes are the prediction results, while the green bounding boxes are the ground truth. Falcon successfully detected objects with occlusions. To point out, Falcon also provided more accurate detections than the original annotations in the last image.

E.10. Task10: Visual Grounding

Visual Grounding

<Description>: A blue vehicle

Q: <CAPTION_TO_PHRASE_GROUNDING> <Description> : Q: [refer] <Description>.

<p style="writing-mode: vertical-rl; transform: rotate(180deg);">Florence-2-L</p> 	<p style="writing-mode: vertical-rl; transform: rotate(180deg);">MiniGPTv2</p> 
<p>Q: Detect an area that matches the description. <Description>. Use horizontal bounding boxes.</p>	
<p style="writing-mode: vertical-rl; transform: rotate(180deg);">Geochat</p> 	<p style="writing-mode: vertical-rl; transform: rotate(180deg);">Llava-1.5</p> 
<p>Q: Detect an area that matches the description. <Description>. Use horizontal bounding boxes.</p>	
<p style="writing-mode: vertical-rl; transform: rotate(180deg);">LHRs-Bot</p> 	<p style="writing-mode: vertical-rl; transform: rotate(180deg);">Sphinx</p> 
<p>Q: Detect an area that matches the description. <Description>. Use horizontal bounding boxes.</p>	
<p style="writing-mode: vertical-rl; transform: rotate(180deg);">Falcon</p> 	

Figure XV. Qualitative comparisons in the task of visual grounding.

Visual Grounding

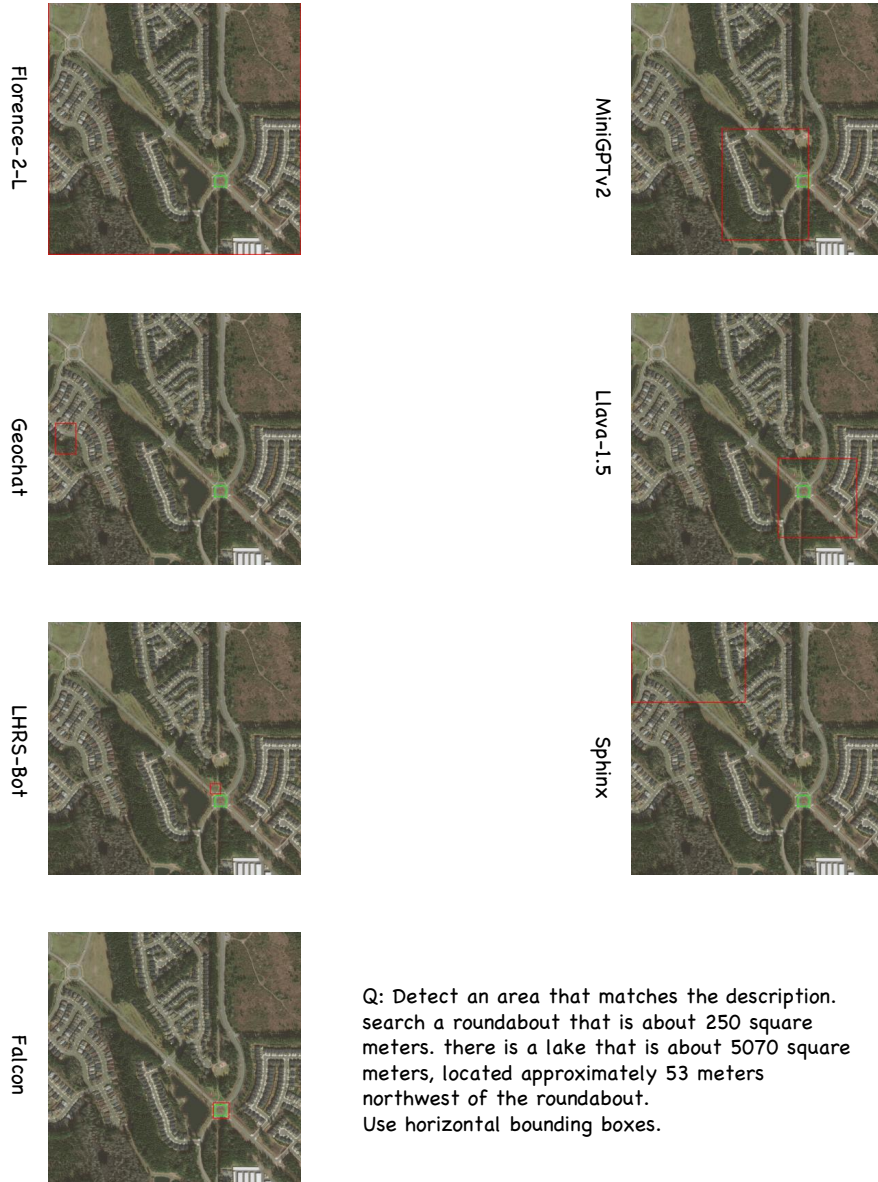


Figure XVI. Qualitative comparisons in the task of visual grounding.

E.11. Task11: Region Captioning

Region Caption			
	<p>Q: Describe the <code><box><88><40><205><199></box></code> in this image.</p>  <p>GT : A small expressway service area.</p>	<p>Q: Describe the <code><box><394><448><634><729></box></code> in this image.</p>  <p>GT : The small overpass in the middle.</p>	<p>Q: Describe the <code><box><245><144><611><886></box></code> in this image.</p>  <p>GT: The ground track field in the middle.</p>
Sphinx	<p>A: The image is a satellite view of a town situated in a valley surrounded by mountains. The town is located near a highway, which can be seen running through the valley. The satellite view provides a clear view of the town's layout, including the buildings and streets. The town appears to be quite large, with a mix of structures and greenery, creating a picturesque scene.</p> <p style="text-align: right;">⊗</p>	<p>A: The image is an aerial view of a highway intersection, showing a roundabout with multiple lanes. There are several cars visible in the scene, with one car located near the top left corner, another in the middle left, and a third car in the middle right area. The cars are driving in different directions, indicating that the intersection is busy.</p> <p style="text-align: right;">⊗</p>	<p>A: The image is an aerial view of a neighborhood, showing a football field and houses. The football field is located in the middle of the scene, surrounded by houses on all sides. The field is marked with white lines, indicating its purpose as a playing area.</p> <p style="text-align: right;">⊗</p>
MiniGPT-v2	<p>A: the new airport</p> <p style="text-align: right;">⊗</p>	<p>A: a wooden bridge</p> <p style="text-align: right;">⊗</p>	<p>A: the football field</p> <p style="text-align: right;">⊗</p>
Florence-2-L	<p>A: building</p> <p style="text-align: right;">⊗</p>	<p>A: highway</p> <p style="text-align: right;">⊗</p>	<p>A: football field</p> <p style="text-align: right;">⊗</p>
Falcon	<p>A: The expressway service area is on the upper left of the bridge on the right.</p> <p style="text-align: right;">✔</p>	<p>A: A overpass is on the left of the red vehicle.</p> <p style="text-align: right;">✔</p>	<p>A: A large oval ground track field in the middle.</p> <p style="text-align: right;">✔</p>

Figure XVII. Qualitative comparisons in the task of region captioning.

E.12. Task12: Pixel Classification

Pixel Classification

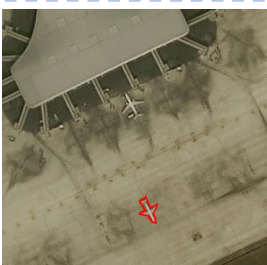
Sample 1		<p>Q: Classify the region of <code><poly><800><839><786><836><779><867><795><869></poly></code>. Use one or a few words.</p> <p>Osprey: Top of a hill. ✘</p> <p>Falcon: Building. ✔</p> <p>Ground truth: Building.</p>
Sample 2		<p>Q: Classify the region of <code><poly><166><502><273><348><290><318><170><294><39><498><161><526></poly></code>. Classes: water area, railway station, road, shipping yard, grassland, residential area, farmland, forest, square, building. Use one or a few words.</p> <p>Osprey: Category of a field is called a field. ✘</p> <p>Falcon: Forest. ✔</p> <p>Ground truth: Forest.</p>
Sample 3		<p>Q: Classify the region of <code><poly><1000><905><0><996><0><1000><113><1000><1000><920></poly></code>. Classes: water area, railway station, road, shipping yard, grassland, residential area, farmland, forest, square, building. Use one or a few words.</p> <p>Osprey: Green and white field. ✘</p> <p>Falcon: Road. ✔</p> <p>Ground truth: Road.</p>
Sample 4		<p>Q: Classify the region of <code><poly><555><891><552><864><503><761><520><773><586><732><479><518><460><508><394><551><404><579><386><570><354><598><481><824><512><904><542><907></poly></code>. Use one or a few words.</p> <p>Osprey: Car (Automobile) . ✘</p> <p>Falcon: Vehicle. ✔</p> <p>Ground truth: Vehicle.</p>
Sample 5		<p>Q: Classify the region of <code><poly><577><804><568><766><584><734><556><747><538><706><517><723><537><757><515><770><547><778><564><801></poly></code>. Classes: baseball field, basketball court, roundabout, excavator, bridge, tennis court, airplane, football field, ship, vehicle, intersection. Use one or a few words.</p> <p>Osprey: Lines. ✘</p> <p>Falcon: Airplane. ✔</p> <p>Ground truth: Airplane.</p>

Figure XVIII. Qualitative comparisons in the task of pixel classification.

E.13. Task13: Segmentation

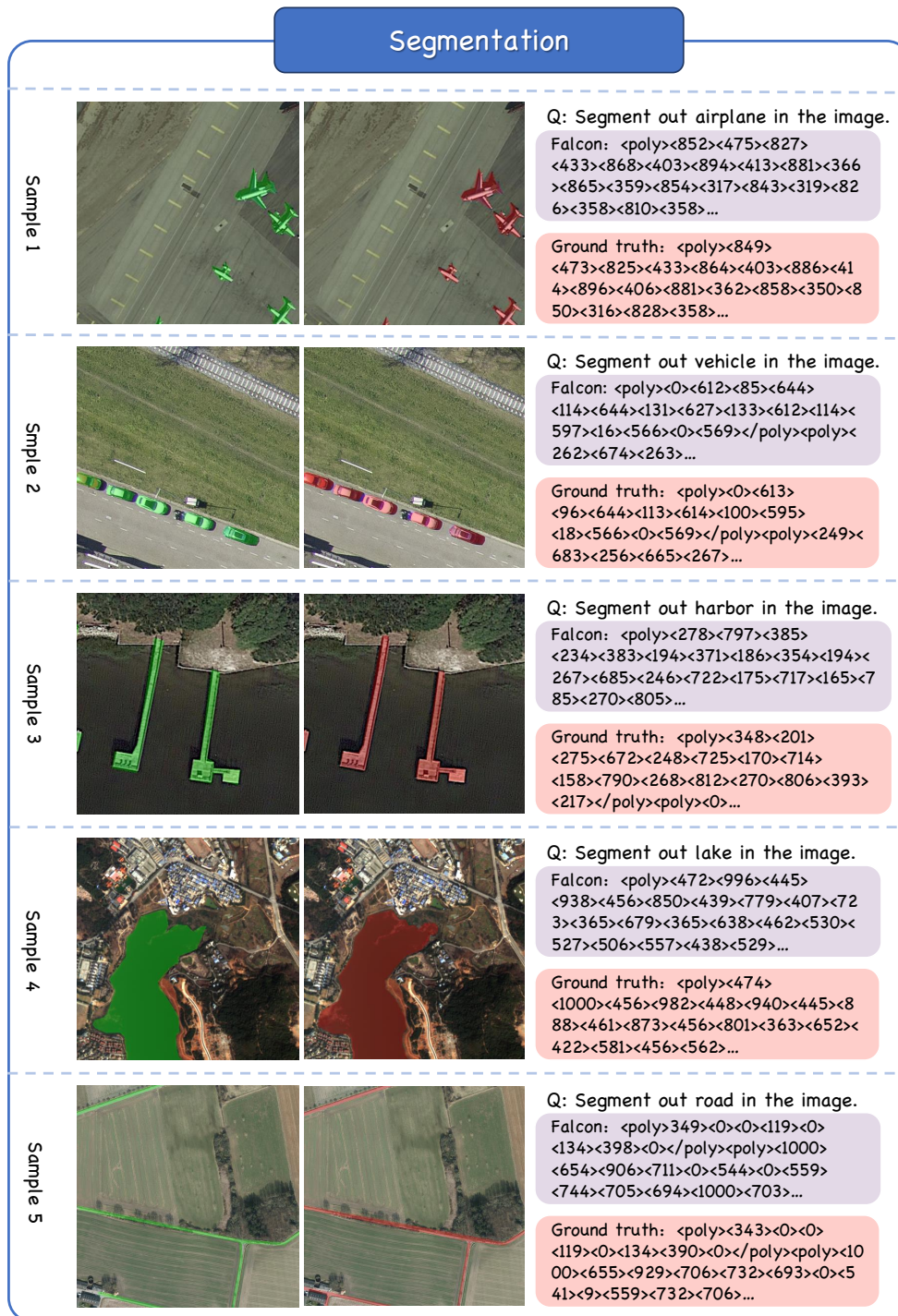


Figure XIX. Qualitative results from Falcon in the task of segmentation.

E.14. Task14: Change Detection

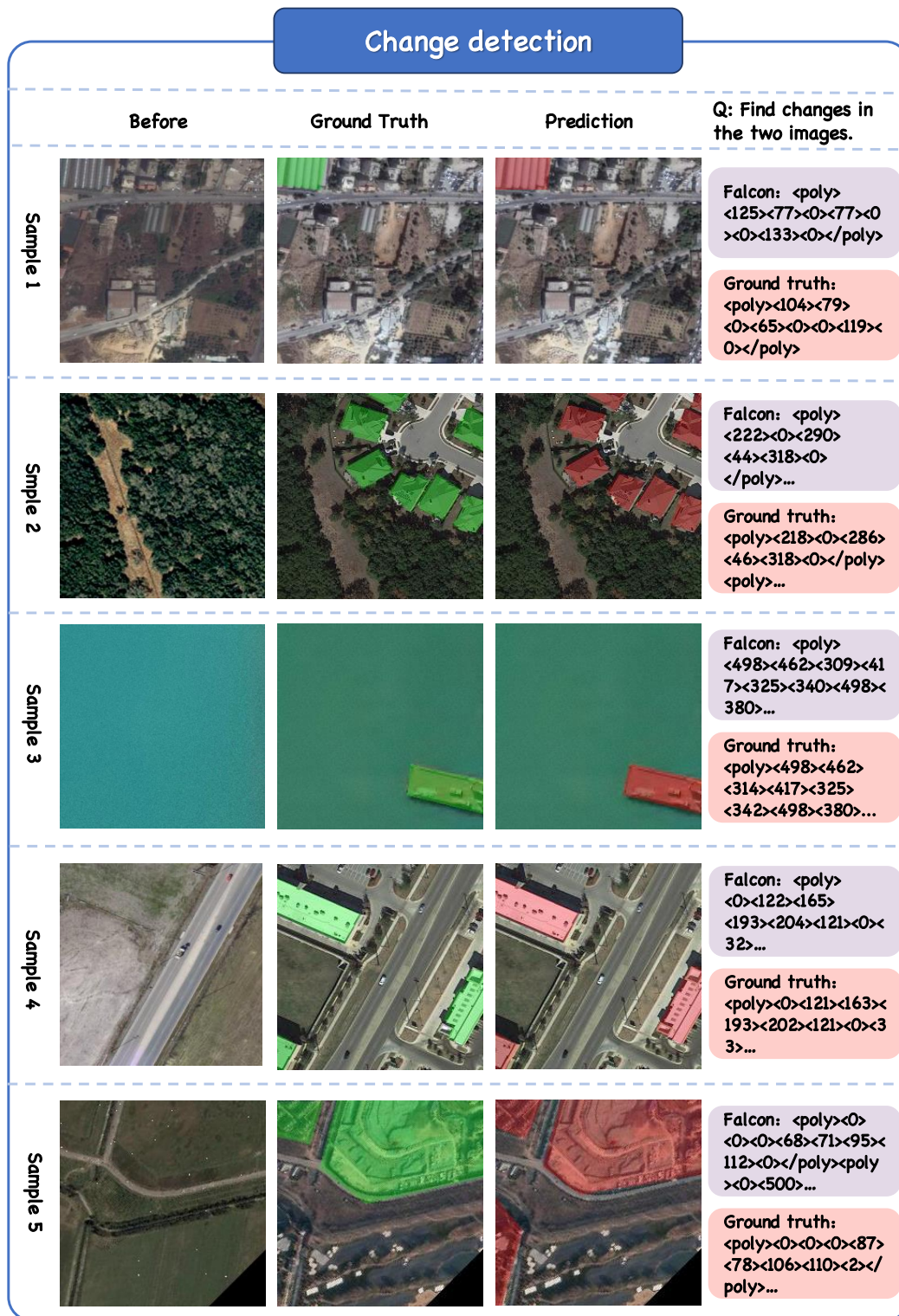


Figure XX. Qualitative results from Falcon in the task of change detection.

F. Quantitative comparison results for remaining tasks

In this section, we first presented the performance of Falcon over image captioning and detailed image captioning tasks (*c.f.* Tab. V), region classification tasks (*c.f.* Tab. VI), visual grounding tasks (*c.f.* Tab. VII) and image region caption tasks (*c.f.* Tab. VIII). As shown in Tab. V to Tab. VIII, general VLMs, such as MiniGPTv2 [101] and Qwen-VL-Chat [3] encountered obstacles in performing effectively on remote sensing data, since they usually lacked the expert knowledge of this domain. Meanwhile, compared with VLMs specialized in remote sensing [27, 51], Falcon achieved better performance in all related datasets, with only 0.7B parameters. Besides, we also provided detailed task performance of region classification with oriented bounding box, object detection with oriented bounding box, semantic segmentation and change detection in Tab. IX, Tab. X, Tab. XI and Tab. XII.

Models	#params	Image caption (CIDEr)				Detailed image caption (CIDEr)		
		RSICD	RSICap	RSITMD	Sydney_Captions	RSICD	RSICap	RSITMD
MiniCPM-V[20]	3B	0.000	0.000	0.000	0.000	0.001	0.547	0.005
MiniGPT-v2[101]	7B	12.212	5.763	9.990	9.971	0.010	0.003	0.112
Florence-2-L[81]	0.7B	10.107	4.733	8.262	6.948	0.562	0.801	1.849
LLaVA-1.5[38]	7B	0.001	0.000	0.000	0.000	0.512	2.120	0.037
Qwen-VL-Chat[3]	7B	7.603	8.275	8.660	8.871	1.070	3.118	3.896
Sphinx[36]	7B	0.001	0.000	0.000	0.000	0.773	1.368	0.723
GeoChat[27]	7B	0.342	1.653	0.418	0.415	2.243	5.191	3.695
LHRS-Bot[51]	7B	4.492	5.222	3.588	12.810	16.195	6.119	16.956
Falcon(Ours)	0.7B	107.070	58.111	32.323	227.564	39.819	26.009	41.905

Table V. A comparison of image captioning performance and detailed image captioning performance on several datasets with 7B+ generic and remote sensing VLMs.

Models	#params	Region level(with horizontal bounding box)							Pixel level						
		DIOR	DOTA2.0	HRSC2016	RSOD	UCAS-AOD	VHRShips	xView	BHP	Watertanks	GEONRW	Globe230k	LoveDA	SAMRS	iSAID
MiniGPT-v2[101]	7B	0.579	0.647	0.821	0.702	0.873	0.825	0.465	-	-	-	-	-	-	-
Florence-2-L[81]	0.7B	0.433	0.731	0.461	0.712	0.939	0.369	0.811	-	-	-	-	-	-	-
Sphinx[36]	7B	0.174	0.106	0.549	0.505	0.389	0.482	0.021	-	-	-	-	-	-	-
Osprey[87]	7B	-	-	-	-	-	-	-	0.009	0.060	0.123	0.076	0.258	0.276	-
Falcon(Ours)	0.7B	0.982	0.998	0.999	0.998	0.999	0.999	0.972	0.999	0.908	0.872	0.813	0.834	0.973	-

Table VI. A comparison of region classification performance (Accuracy) on several datasets with 7B+ generic and remote sensing VLMs.

Models	#params	AP@IoU=0.5(%)	
		DIOR-RSVG	RSVG
MiniGPT-v2[101]	7B	29.892	1.771
Florence-2-L[81]	0.7B	16.929	1.320
LLaVA-1.5[38]	7B	12.085	0.165
Qwen-VL-Chat[3]	7B	31.528	3.627
Sphinx[36]	7B	0.939	0.000
GeoChat[27]	7B	21.024	0.741
LHRS-Bot[51]	7B	11.826	1.318
Falcon(Ours)	0.7B	87.539	56.878

Table VII. A comparison of visual grounding performance with horizontal bounding box on several datasets with 7B+ generic and remote sensing VLMs.

Models	#params	DIOR-RSVG				RSVG			
		Bleu-4	Meteor	Rouge_L	CIDEr	Bleu-4	Meteor	Rouge_L	CIDEr
MiniGPT-v2[101]	7B	1.583	0.105	21.358	17.480	0.000	0.037	10.454	1.588
Florence-2-L[81]	0.7B	0.000	0.033	8.956	5.459	0.000	0.003	1.008	0.349
Sphinx[36]	7B	0.000	0.163	7.535	0.329	0.382	0.166	11.781	0.220
Falcon(Ours)	0.7B	45.294	0.675	62.932	440.809	24.891	0.477	51.242	99.485

Table VIII. A comparison of image region caption performance with horizontal bounding box on several datasets with 7B+ generic and remote sensing VLMs.

Models	#params	Accuracy				
		DIOR	DOTA2.0	FAIR1M1.0	SODA-A	UCAS-AOD
Falcon(Ours)	0.7B	0.981	0.997	0.999	0.974	0.999

Table IX. Region classification performance with oriented bounding box of Falcon.

Models	#params	AP@IoU=0.5(%)															
		ASD	BHP Watertanks	DIOR	DOTA2.0	FAIR1M1.0	GEONRW	Globe230k	LoveDA	S2-SHIPS	SODA-A	SZTAKI	ShipRS	UCAS-AOD	airplane_det	iSAID	ship_det
Falcon(Ours)	0.7B	89.383	78.563	55.299	23.293	60.751	21.720	22.930	36.498	20.758	7.013	20.869	59.936	88.219	83.088	28.832	21.667

Table X. Object detection performance with oriented bounding box of Falcon.

Models	#params	mIoU					
		BHP Watertanks	GEONRW	Globe230k	LoveDA	SAMRS	iSAID
Falcon(Ours)	0.7B	0.684	0.473	0.521	0.435	0.754	0.517

Table XI. Semantic segmentation performance of Falcon.

Models	#params	mIoU								
		DSFIN	EGY_BCD	HRSCD	LEVIR-CD+	LEVIR-CD	MSBC	MSOSCD	S2Looking	SYSU-CD
Falcon(Ours)	0.7B	0.575	0.554	0.341	0.570	0.699	0.384	0.474	0.570	0.561

Table XII. Change detection performance of Falcon.

G. Qualitative comparisons using diversified instructions

In this section, we show that Falcon can understand diversified instructions to perform each task, highlighting its instruction-following capabilities. The results are in Figure XXI and Figure XXII.

Image Caption (Multi-instructions)			
Ground Truth	 <p>rows of houses are located on the left hand of the road while two tennis courts are on the other hand. a road between many buildings and two badminton fields.</p>	 <p>on the ground with a lake. beside the lake there is a forest. many green trees and a road are in two sides of a pond.</p>	 <p>An intersection with some cars on the road. An intersection only with some houses and plants at the corners. An intersection with two roads vertical to each other.</p>
Instruction 1	<p>Q: Describe this image.</p> <p>A: two tennis courts are near a crossroads and many buildings.</p>	<p>A: many green trees are around an irregular pond near a road.</p>	<p>A: some cars are in a crossroads with several buildings.</p>
Instruction 2	<p>Q: Introducing this image.</p> <p>A: two tennis courts are near a crossroads and many buildings.</p>	<p>A: many green trees are around an irregular pond near a road.</p>	<p>A: some cars are in two sides of a crossroads with several buildings.</p>
Instruction 3	<p>Q: Explain what you see in this image.</p> <p>A: two tennis courts are near a crossroads and many buildings.</p>	<p>A: many green trees are around an irregular pond near a road.</p>	<p>A: several buildings are near a crossroads with many cars.</p>
Instruction 4	<p>Q: What does this image show?</p> <p>A: two tennis courts are near many buildings.</p>	<p>A: many green trees are around an irregular pond near a road.</p>	<p>A: several buildings are near a crossroads with many cars.</p>

Figure XXI. Qualitative comparisons using diversified instructions in the task of image captioning.

Region Detection-HBB (Multi-instructions)

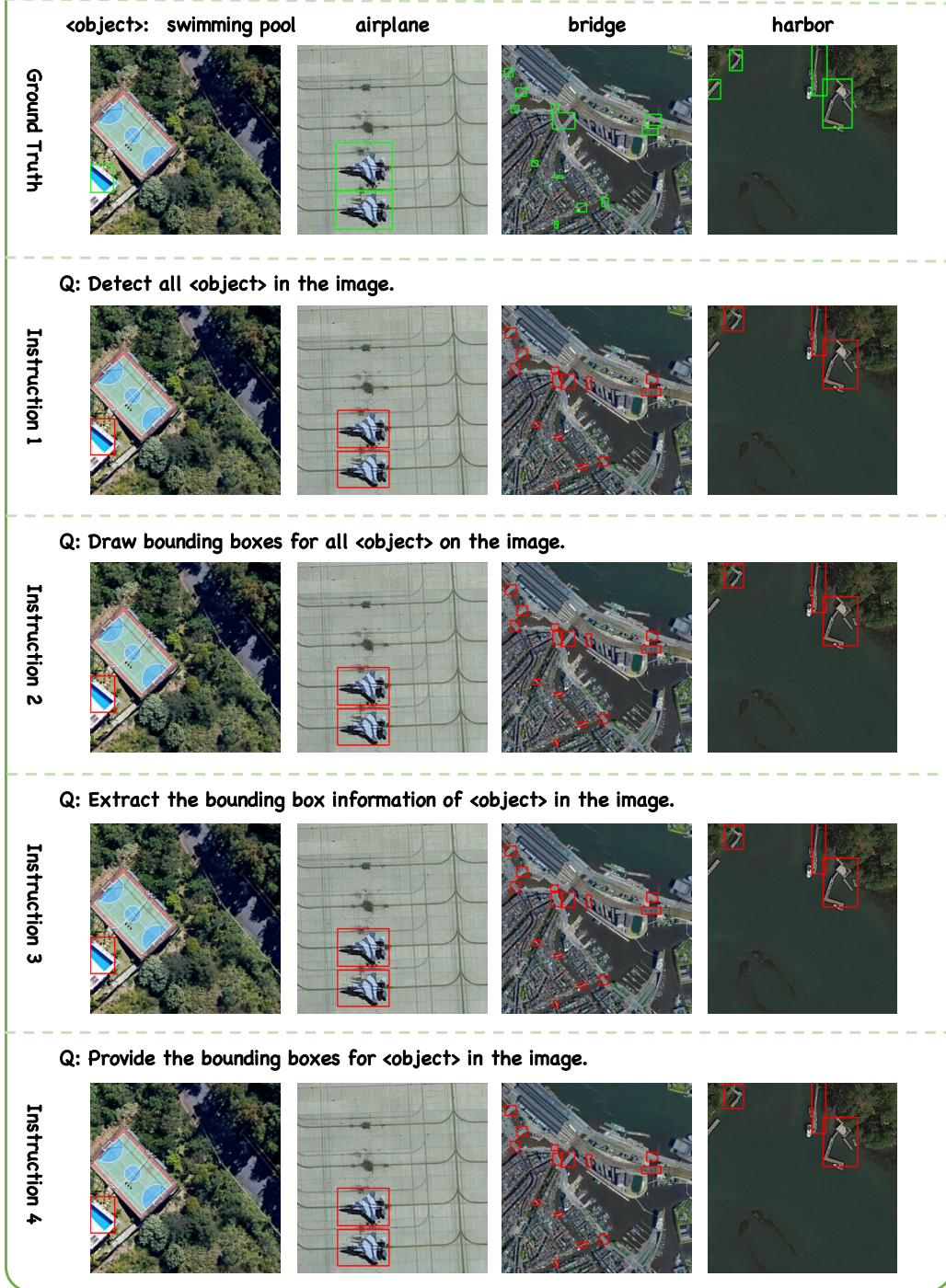


Figure XXII. Qualitative comparisons using diversified instructions in the task of Region Detection-HBB.

H. Experiment setup for human evaluation

Here we provide more details for the human evaluation described in Sec 5.1. We selected 50 images of various types from Falcon_SFT dataset, including diverse scenes such as urban, rural, and industrial areas, covering amount of labels such as roads, grasslands, buildings, ponds, and farmlands, etc. To ensure the accuracy and reliability of the evaluation, we invited ten volunteers to assess the models’ image captioning performance. They were presented with the images, instruction and model responses, with all the model information anonymized. Following [21], the generated image captions were scored from three dimensions, i.e. detail, position and hallucination description. Each dimension was rated with a four-level rating system as A, B, C, and D. The specific criteria for each level are shown in Tab. XIII.

The detailed scoring results are shown in Tab. 6 and Fig. XXIII. By quantifying the A-D ratings as 4 to 1 points, our model Falcon achieved the highest average scores across all three dimensions, with scores of 3.274, 3.426, and 2.988, respectively. As shown in the Fig. XXIII, Falcon received the fewest C and D ratings and the most A and B ratings across all three dimensions. Although Falcon received fewer A ratings than Qwen in the hallucination dimension, examples in Fig. XXIV reveal that the outputs of Qwen are overly simplistic. While they avoid hallucination issues, they lack detailed descriptions and accurate positional information. Overall, Falcon consistently outperformed other models, receiving the highest scores in the quantitative analysis and providing the most detailed and accurate descriptions in the qualitative comparison.

Dimension	Level	Description
Detail	A	The caption has comprehensive and rich details, describing almost all types of objects in the ground truth.
	B	The caption has rich details, describing most types of objects and their attribute information.
	C	The caption has only a small amount of details, describing a few types of objects and their attribute information.
	D	The caption has no detail descriptions.
Position	A	The caption has rich position descriptions for objects and all are correct.
	B	The caption has rich position descriptions for objects with an accuracy higher than 50%.
	C	The caption has few position descriptions, or rich position descriptions but with an accuracy less than 50%.
	D	The caption has no position descriptions.
Hallucination	A	The caption has no hallucination description.
	B	The caption has hallucination description, and it accounts for less than 50%
	C	The caption has a large proportion of hallucination description, more than 50%
	D	The caption is entirely hallucination description.

Table XIII. Caption Evaluation Criteria

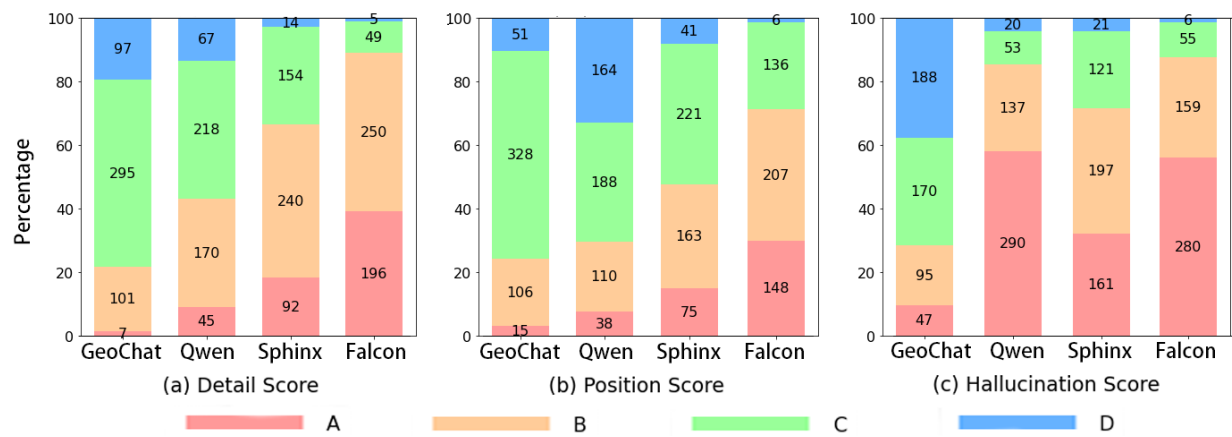


Figure XXIII. Human evaluation among generic and remote sensing VLMs on image captioning task.

	[Instruction]	Describe the image in detail.	Rank				
	[Model Response]			A	B	C	D
	GeoChat	The image depicts a cityscape with various buildings and structures. There are two buildings close to each other at the top left corner of the image. At the top right corner, there are two buildings close to each other. In the center of the image, there are two buildings close to each other. Additionally, there are two buildings at the bottom left corner of the image.	D	0	1	7	2
			P	0	3	7	0
			H	1	2	5	2
	Qwen	This is an aerial view of a factory. On the left side of the image, there is a blue and white building. In the middle of the image, there is a black building with many small squares on its roof. To the right of the black building, there is a brown building with a green roof.	D	0	3	7	0
			P	0	4	6	0
			H	2	7	1	0
	Sphinx	The image is an aerial view of a large industrial area with several buildings and a parking lot. The buildings are arranged in a way that creates a pattern, with some buildings being larger and others smaller. The parking lot is located in the middle of the industrial area, surrounded by the buildings.	D	1	4	5	0
			P	3	2	5	0
			H	2	1	7	0
	Falcon	This satellite image mainly shows a large industrial facility, surrounded by farmland and some residential areas. This facility consists of multiple rectangular buildings, which may be warehouses or production facilities. The colors of these buildings are mainly gray and blue, and some also have white roofs. In addition, there is a farmland in the lower right corner of the image, which shows green and yellow hue. There are a large number of rectangular buildings in the image for industrial production activities. There is a large area of farmland on the right side of the picture, which is mainly used for agricultural production.	D	6	4	0	0
			P	5	2	3	0
			H	7	3	0	0
	[Instruction]	Describe the image in detail.	Rank				
	[Model Response]			A	B	C	D
	GeoChat	The image depicts a rural scene with a single building located at the center of the image. The building appears to be surrounded by trees, with some trees located at the bottom left and bottom right of the image. The building is likely a farmhouse or a small village structure, and the trees provide a serene and natural backdrop to the scene.	D	0	5	5	0
			P	0	8	2	0
			H	3	5	1	1
	Qwen	A satellite image of a rural area with a road cutting through it. The road is marked with white lines.	D	0	1	9	0
			P	0	1	6	3
			H	5	5	0	0
	Sphinx	The image is an aerial view of a green forest, captured from a satellite or a plane. The forest is filled with trees, and a road can be seen cutting through the landscape. The road appears to be a dirt road, and it is surrounded by the lush greenery.	D	4	5	1	0
			P	4	3	1	0
			H	3	6	1	0
	Falcon	This satellite image captures a hill terrain covered by the forest, and there are some houses and roads scattered. These houses are mainly concentrated in the center of the image, surrounded by dense green trees. The whole scene gives people a quiet rural life, and people live in harmony with nature. This area is mainly composed of dense forests, occupying most of the images. There are several houses in the image scattered on the hillside, which may be the residence of local residents.	D	5	4	1	0
			P	5	4	1	0
			H	7	3	0	0

Figure XXIV. The qualitative comparison among GeoChat, Qwen, Sphinx, and Falcon on the proposed image captioning test set. The number of ratings for detail (D), position (P), and hallucination (H) description is shown in the ‘Rank’ columns.

I. More ablation experiments

This section presents more ablation study results, expecting to demonstrate the effectiveness of our proposed Falcon_SFT dataset. Specifically, as shown in Fig. XXV, we finetune the GeoChat and LLaVA-1.5 on the Falcon_SFT dataset using LoRA. The performance trends during the first 9000 training steps indicate that the Falcon_SFT dataset enables the current best models to continue improving their performance.

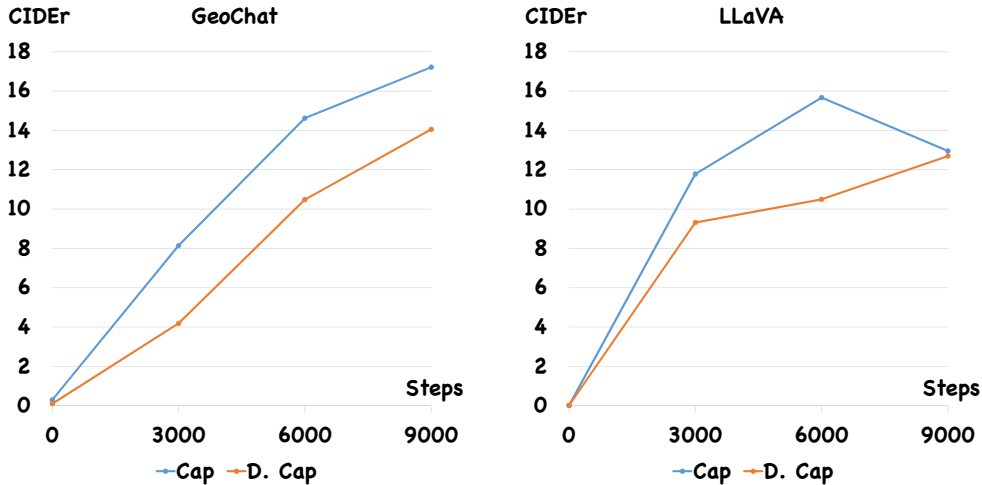


Figure XXV. Lora fine-tuning of GeoChat and LLaVA-1.5 on Falcon_SFT.

Additionally, we conducted experiments to verify that Falcon learned robust and generalizable representations. To this end, we evaluated the model’s zero-shot performance while progressively increasing the training data scale. As shown in Tab. XIV, Falcon effectively avoided overfitting, demonstrating its ability to learn stable and transferable representations rather than merely memorizing the training data.

Data Scale	Cap (CIDEr)	Cls (Accuracy)	Count (Accuracy)			Seg (mIoU)
	UCM-Captions	AID	LRBEN	MAR20	NWPU-VHR-10	GID15
10%	23.630	0.213	0.235	0.809	0.754	0.347
50%	26.360	0.252	0.223	0.820	0.786	0.378
100%	30.481	0.363	0.252	0.876	0.798	0.390
Data Scale	D.Cap (CIDEr)	Det ^{hbb} (AP@IoU=0.5)			Det ^{obb} (AP@IoU=0.5)	
	UCM-Captions	GID15	MAR20	NWPU-VHR-10	GID15	MAR20
10%	13.343	17.436	92.574	77.666	9.866	77.930
50%	28.500	19.632	92.260	80.771	11.232	82.370
100%	23.554	23.548	94.189	80.678	16.297	83.270

Table XIV. Ablation studies on zero-shot performance of Falcon with increasing training data scale.

Finally, we conduct ablation experiments on the choice of encoder-decoder architecture over the decoder-only architecture. To this end, decoder-only architectures, such as MiniCPM-V [20], typically require a large and computationally intensive LLM. We believe this type of module is not essential for remote sensing vision tasks and may introduce unnecessary computational overhead. As shown in Table XV, after fine-tuning Falcon and MiniCPM-V [20] on the same dataset (a subset of FCD), we observed similar performance. Notably, Falcon has fewer parameters, which makes it more suitable for deployment.

Models	Det ^{hbb}		Det ^{obb}		Cap		Cls		VQA		VG
	AP@IoU=0.5		Precision@IoU=0.5		Rouge_L		Accuracy		Accuracy		AP@IoU=0.5
	DIOR	DOTA2.0	DIOR	DOTA	RSICD	RSITMD	AID	EuroSAT	HRBEN	LRBEN	DIOR-RSVG
Decoder-Only (MiniCPM-V [20])	40.277	36.440	0.533	0.454	0.474	0.290	0.984	0.971	0.816	0.740	0.749
Encoder-Decoder (Falcon)	53.666	48.262	0.886	0.831	0.507	0.361	0.987	0.975	0.817	0.752	0.871

Table XV. Ablation studies on the choice of encoder-decoder architecture over the decoder-only architecture.

J. Evaluation metric for each task

J.1 Accuracy

In our image classification task, we aim to ensure consistent and fair comparisons across different datasets and models, which is challenging due to variations in label naming and class hierarchies in datasets and models. To address this, we leverage BERT (Bidirectional Encoder Representations from Transformers), a powerful language model, to standardize the mapping of classification results into the specific remote sensing classes of each dataset. BERT is well-suited for this task because it captures semantic relationships and contextual information in text, making it ideal for aligning class labels that may differ in terminology but share similar meanings. By using BERT to map our classification outputs to consistent class names, we can harmonize class labels across models with different naming conventions or granularities, ensure that semantically similar classes are mapped together, reducing discrepancies in label interpretation, and improve the interpretability of results, especially in multi-source, multi-dataset, multi-model evaluations.

For evaluating classification performance, we use accuracy as our primary evaluation metric, defined as follows:

$$\text{Accuracy} = \frac{\text{Number of Correct Predictions}}{\text{Total Number of Predictions}} = \frac{TP + TN}{TP + TN + FP + FN} \quad (\text{S1})$$

where TP (True Positives) and TN (True Negatives) are the counts of correctly predicted positive and negative instances, respectively. FP (False Positives) and FN (False Negatives) are the counts of incorrectly predicted positive and negative instances, respectively.

Using BERT for label mapping and accuracy as the evaluation metric allows us to conduct a more reliable and interpretable comparison of model performance across diverse remote sensing datasets.

J.2 BLEU, METEOR, CIDEr, ROUGE-L

To evaluate our captioning performance, we use the following metrics: BLEU, METEOR, CIDEr, and ROUGE-L. These metrics provide a comprehensive assessment of the quality of generated captions by measuring different aspects of caption similarity to reference captions. The equations are as follows:

J.2.1 BLEU (Bilingual Evaluation Understudy)

BLEU measures the precision of n-grams (typically up to 4-grams) between the geROUGE-Lnerated captions and reference captions. It is a precision-oriented metric that does not account for recall.

$$\text{BLEU} = \exp \left(\sum_{n=1}^N w_n \log p_n \right) \times \text{brevity_penalty} \quad (\text{S2})$$

where p_n is the precision of n-grams, w_n is the weight for each n-gram level, and the brevity penalty penalizes shorter generated captions.

J.2.2 METEOR (Metric for Evaluation of Translation with Explicit ORdering)

METEOR considers both precision and recall and uses the harmonic mean (F1 score) of these measures. It includes stemming and synonym matching, making it more robust to variations in word choice.

$$\text{METEOR} = F_{\text{mean}} \times (1 - \text{penalty}) \quad (\text{S3})$$

where F_{mean} is the harmonic mean of precision and recall, and the penalty term penalizes longer, less precise matches.

J.2.3 CIDEr (Consensus-based Image Description Evaluation)

CIDEr measures consensus between generated and reference captions by applying term frequency-inverse document frequency (TF-IDF) weighting, which emphasizes terms that are more descriptive.

$$\text{TF-IDF}(t, s) = \text{TF}(t, s) \times \text{IDF}(t) \quad (\text{S4})$$

$$\text{CIDEr}_n(g, r) = \frac{\sum_{t \in g \cap r} \text{TF-IDF}(t, g) \times \text{TF-IDF}(t, r)}{\sqrt{\sum_{t \in g} (\text{TF-IDF}(t, g))^2} \cdot \sqrt{\sum_{t \in r} (\text{TF-IDF}(t, r))^2}} \quad (\text{S5})$$

$$\text{CIDEr}(g) = \frac{1}{N} \sum_{n=1}^N \frac{1}{|R|} \sum_{r \in R} \text{CIDEr}_n(g, r) \quad (\text{S6})$$

$$\text{CIDEr} = \frac{1}{|G|} \sum_{i=1}^{|G|} \text{CIDEr}(g_i) \quad (\text{S7})$$

where $\text{TF}(t, s)$ is the term frequency of t in s , and $\text{IDF}(t) = \log \frac{N}{1+n(t)}$, with N as the total number of captions and $n(t)$ as the number of captions containing t . R is the set of reference sentences, $|G|$ is the total number of generated captions.

J.2.4 ROUGE-L (Recall-Oriented Understudy for Gisting Evaluation)

The ROUGE-L metric measures the longest common subsequence (LCS) between a generated caption G and a reference caption R . Given $\text{LCS}(G, R)$ as the length of the longest common subsequence, calculated as follows:

$$\text{Recall} = \frac{\text{LCS}(G, R)}{|R|} \quad (\text{S8})$$

$$\text{Precision} = \frac{\text{LCS}(G, R)}{|G|} \quad (\text{S9})$$

$$\text{ROUGE-L} = \frac{(1 + \beta^2) \times \text{Precision} \times \text{Recall}}{\text{Recall} + \beta^2 \times \text{Precision}} \quad (\text{S10})$$

where β is typically set to 1, giving equal importance to precision and recall.

J.3 AP@IoU=0.5

In our object detection and visual grounding tasks, we employ the evaluation metric $\text{AP@IoU=0.5}(\text{AP@50})$ to assess the performance of each model accurately across Horizontal Bounding Box (HBB) detection, Oriented Bounding Box (OBB) detection, and visual grounding. AP@50 is defined as Average Precision (AP) at 50% Intersection over Union (IoU) threshold. It measures the average precision of detections where the IoU between predicted and ground-truth bounding boxes is at least 50%. AP@50 balances precision and recall across different confidence thresholds, providing a summary metric of detection quality. It is calculated as:

$$\text{AP@50} = \frac{1}{|\mathcal{D}|} \sum_{d \in \mathcal{D}} \text{Precision}(d) \times \text{Recall}(d) \quad (\text{S11})$$

where \mathcal{D} is the set of detections, and Precision and Recall are computed at an IoU threshold of 0.5. AP@50 gives an overall measure of how well the model detects objects with minimal overlap criteria.

J.4 mIoU

In our segmentation and change detection tasks, we employ mean Intersection over Union (mIoU) as the evaluation metric. mIoU is widely used in semantic segmentation and change detection tasks as it provides a comprehensive assessment of the model’s ability to correctly predict class boundaries across the entire dataset. The mIoU is defined as follows:

Mean Intersection over Union (mIoU) The mIoU measures the overlap between predicted and ground-truth regions for each class, averaged over all classes. It is computed as:

$$\text{mIoU} = \frac{1}{C} \sum_{c=1}^C \frac{\text{TP}_c}{\text{TP}_c + \text{FP}_c + \text{FN}_c} \quad (\text{S12})$$

where C is the total number of classes, TP_c (True Positives) represents the correctly predicted pixels for class c , FP_c (False Positives) represents the pixels incorrectly predicted as class c , FN_c (False Negatives) represents the pixels of class c that were not correctly predicted.

In segmentation, mIoU evaluates the overlap quality of predicted regions with respect to the ground truth for each class, making it an effective metric for measuring model performance in pixel-wise classification. For change detection, mIoU helps quantify the accuracy of predicted change regions by comparing the overlap between predicted change areas and actual

change areas in the ground truth. This metric is particularly useful in remote sensing applications where precise boundary alignment is essential for detecting changes over time. Using mIoU for both segmentation and change detection allows us to assess how well the model captures class-specific and change-specific information, providing a reliable measure of performance in spatially complex remote sensing tasks.